



ARTICLE

LncRNA-encoded polypeptide ASRPS inhibits triple-negative breast cancer angiogenesis

Yirong Wang^{1*}, Siqi Wu^{1*}, Xun Zhu^{2*}, Liyuan Zhang^{3*}, Jieqiong Deng¹, Fang Li¹, Binbin Guo¹, Shenghua Zhang¹, Rui Wu¹, Zheng Zhang¹, Kexin Wang¹, Jiachun Lu⁴ , and Yifeng Zhou¹ 

Triple-negative breast cancer (TNBC) is a subtype of breast cancer (BC) with the most aggressive phenotype and poor overall survival. Using bioinformatics tools, we identified *LINC00908* encoding a 60-aa polypeptide and differentially expressed in TNBC tissues. We named this endogenously expressed polypeptide ASRPS (a small regulatory peptide of STAT3). ASRPS expression was down-regulated in TNBCs and associated with poor overall survival. We showed that *LINC00908* was directly regulated by ER α , which was responsible for the differential down-regulation of *LINC00908* in TNBCs. ASRPS directly bound to STAT3 through the coiled coil domain (CCD) and down-regulated STAT3 phosphorylation, which led to reduced expression of VEGF. In human endothelial cells, a mouse xenograft breast cancer model, and a mouse spontaneous BC model, ASRPS expression reduced angiogenesis. In a mouse xenograft breast cancer model, down-regulation of ASRPS promoted tumor growth, and ASRPS acted as an antitumor peptide. We presented strong evidence that *LINC00908*-encoded polypeptide ASRPS represented a TNBC-specific target for treatment.

Introduction

Triple-negative breast cancer (TNBC) does not express the three most common breast cancer (BC) markers, estrogen receptor (ER), progesterone receptor, and *HER2/neu* oncogene (HER2), and belongs to the basal-like BC type by gene expression profile (Elias, 2010). In the United States, TNBC accounts for 10–15% of all BCs, and is more common in women of African descent and in women <50 yr old (Brewster et al., 2014). The incidence of BC in China has been increasing at a rate of 3.5% per year since 2000. It was estimated that there were 268,600 new BC cases and 69,500 deaths from BC in China in 2015 (Chen et al., 2016). With current annual rate of increase, it is projected that by 2021, there would be 2.5 million cases of BC in China. About 20% of BCs in China are TNBC subtype (Peng et al., 2016). TNBC is the most aggressive subtype of BC and is associated with worst prognosis and overall survival (OS; Son et al., 2019). It is characterized by high cell proliferation, poor cellular differentiation, and more frequent disease recurrence (Chang et al., 2018). Compared with non-TNBC, TNBC patients have poor prognosis, including higher nuclear grade, increased incidence of lung and brain metastases, and shorter recurrence-free interval. Further, TNBC patients do not benefit from endocrine therapy or HER2-targeted therapy (Foulkes et al., 2010), and TNBC patients demonstrate enhanced

angiogenesis when compared with non-TNBC patients (Ribatti et al., 2016). Despite the fact that significant improvement has been made for BC treatment, treatment options for TNBC are limited, including surgery, radiotherapy, and chemotherapy. No targeted therapies are available for TNBC. Elucidating the tumorigenesis in TNBC is key to developing TNBC-specific therapies and improving patients' OS.

Long noncoding RNAs (lncRNAs) are nonprotein coding transcripts longer than 200 nucleotides. Recent studies have shown that lncRNAs participate in cancer initiation and progression (Kong et al., 2018). Aberrant expression of lncRNAs has been observed in various types of cancer, including BC. LncRNAs can act as either tumor-suppressor genes or oncogenes (Li et al., 2019; Wu et al., 2015), and regulate cell proliferation and invasion (Li et al., 2017). Mechanistically, lncRNAs serve as transcription regulators through different modes. They can act as signal RNAs to regulate transcription in response to various stimuli; they can act as decoy RNAs to limit the availability of regulatory factors; they can act as scaffold RNAs to provide platforms for assembling protein complexes for transcription; they can act as guide RNAs for the proper localization of ribonucleoproteins; and they can act as enhancer RNAs for

¹Department of Genetics, Medical College of Soochow University, Suzhou, China; ²Department of General Surgery, The Second Affiliated Hospital of Soochow University, Suzhou, China; ³Department of Radiotherapy and Oncology, The Second Affiliated Hospital of Soochow University, Suzhou, China; ⁴The State Key Lab of Respiratory Disease, The First Affiliated Hospital, The School of Public Health, Guangzhou Medical University, Guangzhou, China.

*Y. Wang, S. Wu, X. Zhu, and L. Zhang contributed equally to this paper; Correspondence to Yifeng Zhou: zhouyifeng@suda.edu.cn.

© 2019 Wang et al. This article is distributed under the terms of an Attribution–Noncommercial–Share Alike–No Mirror Sites license for the first six months after the publication date (see <http://www.rupress.org/terms/>). After six months it is available under a Creative Commons License (Attribution–Noncommercial–Share Alike 4.0 International license, as described at <https://creativecommons.org/licenses/by-nc-sa/4.0/>).

chromatin interactions (Fang and Fullwood, 2016). More recently, it has also been shown that some noncoding RNAs function through their encoding polypeptides (Ingolia et al., 2011). Notably, an 87-aa tumor suppressive peptide encoded by the circular form of long intergenic nonprotein-coding RNA could directly interact with polymerase associated factor complex and inhibit the transcriptional elongation in glioblastoma (Zhang et al., 2018); *Circ-AKT3* encodes a 174-aa novel protein that is a negative regulator of the receptor tyrosine kinase/PI3K pathway (Xia et al., 2019). A polypeptide named SPAR (small regulatory polypeptide of amino acid response), encoded by *LINC00961*, can regulate mTORC1 and muscle regeneration (Matsumoto et al., 2017); lncRNA *HOXB-AS3* encodes a peptide suppressing colon cancer growth (Huang et al., 2017); myoregulin, encoded by a putative lncRNA, regulates muscle performance (Anderson et al., 2015); a recent study identified CASIMO1, a novel small protein encoding by a small open reading frame (ORF) from lncRNA that interacted with squalene epoxidase and was able to influence lipid droplet formation (Polycarpou-Schwarz et al., 2018).

Recent studies have identified a series of dysregulated lncRNAs in TNBC when compared with adjacent normal tissues (Kong et al., 2018; Rodríguez Bautista et al., 2018). These differentially expressed lncRNAs can be used to classify TNBCs into different subgroups and facilitate the development of targeted therapies (Zhang et al., 2019); they can also be used as prognostic markers for survival and potential therapeutic targets. However, little is known about how these lncRNAs are regulated, and no reports have identified lncRNAs with coding potentials.

In the present study, we identified TNBC-specific lncRNAs from The Cancer Genome Atlas (TCGA) database and predicted the lncRNAs with coding potential using the GWIPS-viz dataset. Subsequently, we showed that one of these TNBC-specific lncRNAs, *LINC00908*, is regulated by ER α , and it contains small ORFs encoding a 60-aa functional polypeptide, a small regulatory peptide of STAT3 (ASRPS), that is involved in TNBC progression. Finally, we determined the signaling pathways regulating the expression of ASRPS as well as downstream STAT3/vascular endothelial growth factor (VEGF) pathways regulated by ASRPS in TNBC.

Results

Identification of TNBC-specific *LINC00908*

To identify TNBC-specific lncRNAs, we first searched for lncRNAs with coding ability, using the following criteria: (1) encoding ORFs by ORFFinder; (2) the ORFs overlapping with the peaks of ribosome profiling data from the GWIPS-viz database. A totally of 583 lncRNAs were identified. Then we looked for lncRNAs that were differentially expressed in TNBC tissues when compared with normal tissues (set A), but not differentially expressed in non-TNBC tissues when compared with normal tissues (set B). A total of 26 candidate lncRNAs were identified (Fig. 1 A). Next, we measured the expression of these 26 lncRNAs by quantitative RT-PCR (qRT-PCR) in 53 pairs of TNBC and adjacent normal tissue samples, and 18 lncRNAs showed differential expression (Fig. 1 B). Of these 18 lncRNAs,

only 10 of them did not show differential expression in 53 pairs of non-TNBC and normal tissue samples (Fig. 1 C). Finally, these 10 lncRNAs were analyzed by polysome profiling and qPCR in MDA-MB-231 and Hs578T cell lines, and only four of them were detected (Fig. 1 D). Using ORFFinder, all putative ORFs longer than 30 aa's in the sense (+) orientation with an initiating ATG codon among these four lncRNAs were predicted (Fig. 1 E and Fig. S1, A–C), and constructed in pcDNA3.1 tagged with FLAG at the C terminal. The plasmids were transfected into TNBC cell line MDA-MB-231, and Western blot analysis indicated that only *LINC00908*-ORF3 translated into a polypeptide (Fig. 1 F and Fig. S1, A–C).

LINC00908 was annotated as an lncRNA in the human genome (NR_015417.1). We analyzed the expression of *LINC00908* in the TCGA database and Cancer Cell Line Encyclopedia project and found that *LINC00908* expression was lower in TNBC tissues or cells compared with non-TNBC tissues or cells (Fig. S1, D and E). *LINC00908* transcript was detected in two pairs of human TNBC tissue samples by Northern blot analysis (Fig. S1 F). Both confocal microscopy analysis of fluorescent in situ hybridization (FISH) and nuclear/cytoplasm fractionation experiment showed that *LINC00908* is a cytoplasmic RNA (Fig. S1, G and H).

LINC00908 encoded a polypeptide

To confirm that *LINC00908* encoded a polypeptide, we inserted a FLAG-tag at the C terminal of the ORF (FLAG-KI), and the polypeptide was detected by immunofluorescence staining using anti-FLAG antibody (Fig. 1 G).

The ORF of *LINC00908* is located on chromosome 18, covering three exons of *LINC00908*, and encodes a 60-aa peptide (6.62KD). The sequence information of the peptide and the region of *LINC00908* encoding peptide are shown in Fig. S1 I. This was consistent with ribosome occupancy data from the GWIPS-viz database (Fig. S1 J). We named this polypeptide ASRPS.

To determine whether the in-frame ATG codon of the ASRPS was functional, we generated a plasmid (ASRPS-GFPmut) by fusing GFPmut ORF (in which the start codon ATGGTG has mutated to ATTGTT) to the C terminus of the ASRPS and transfected it into the MDA-MB-231 cell line (Fig. 1 H). 24 h after transfection, the expression of the GFP fusion protein was observed in MDA-MB-231 cells, suggesting that the ASRPS ATG codon was functional (Fig. 1 I). GFP fusion protein was also detected by Western blot analysis using anti-GFP antibody (Fig. 1 J). On the contrary, GFP fusion protein was not detected when the ATG codon in ASRPS was mutated (ASRPSmut-GFPmut). To rule out effect of the relative large size of GFP on the fusion protein, we also confirmed the functionality of ASRPS start codon by generating FLAG-tag fusion protein in MDA-MB-231 cells. The FLAG fusion protein was detected by both Western blot and immunofluorescence staining using anti-FLAG antibody (Fig. 1, K–M).

ASRPS was expressed endogenously and down-regulated in TNBC

To determine whether ASRPS was endogenously expressed, we performed polysome profiling in MDA-MB-231 cells. The mRNA-protein particles (mRNPs) were separated into three

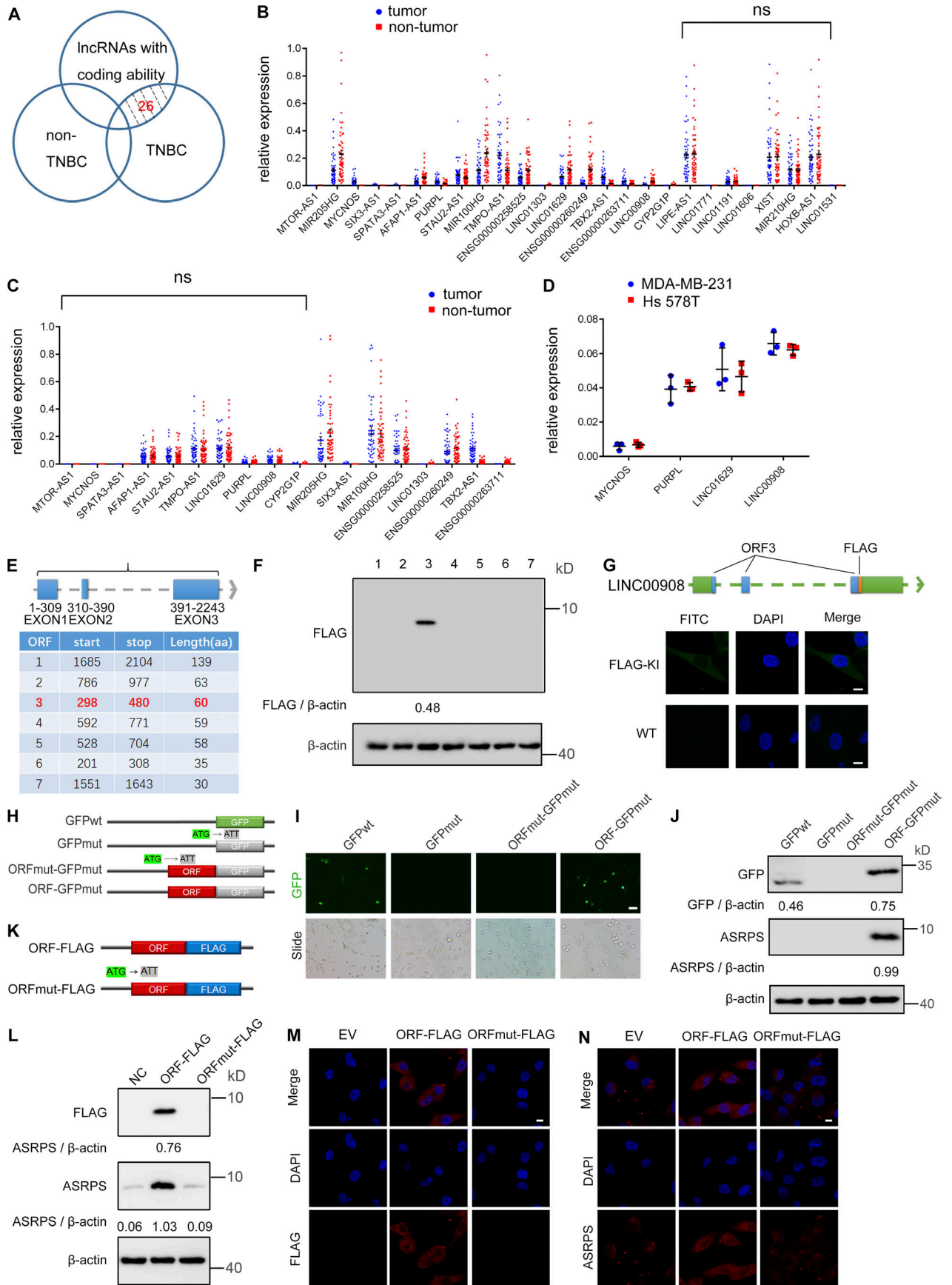


Figure 1. Identification of TNBC-specific *LINC00908* which encoded a polypeptide. (A) The Venn diagram demonstrated the identification of 26 TNBC-specific candidate lncRNAs. (B) Expression of 26 candidate lncRNAs in 54 matched TNBC and nontumorous tissues. 18 of 26 lncRNAs did show differential expression ($n = 54$). (C) Expression of 18 candidate lncRNAs in 54 matched non-TNBC and nontumor tissues. 10 of 18 lncRNAs did not show differential expression ($n = 54$). (D) Four lncRNAs were detected in the polysome fractions from both MDA-MB-231 and Hs578T cell lines ($n = 3$). (E) Genomic locations of seven predicted ORFs of *LINC00908*. (F) The seven ORF-FLAG fusion constructs in pcDNA3.1 were transfected into MDA-MB-231 cells. Each ORF-FLAG fusion protein was detected by Western blot using anti-FLAG antibody 24 h after transfection. (G) Top: Diagram of the ORF3 location at the *LINC00908* locus and the FLAG tag that was inserted to the 3' end of ORF3. Bottom: ORF-FLAG fusion protein levels were determined by immunofluorescence with anti-FLAG antibody in MDA-MB-231 cells (scale bars, 10 μm). (H) Diagram of the GFP fusion constructs. The start codon ATGGTG of the GFP (GFPwt) gene was mutated to ATTGTT (GFPmut). The start codon ATG of the *LINC00908* ORF was mutated to ATT. (I and J) The indicated constructs were transfected into MDA-MB-231 cells. 24 h after transfection, the GFP fluorescence was detected using fluorescence microscope (scale bars, 100 μm ; I), and fusion protein levels were determined by Western blot with anti-GFP and ASRPS antibodies, respectively (J). (K) Diagram of the FLAG fusion constructs. The start codon ATG of the *LINC00908* ORF was mutated to ATT. (L–N) The indicated constructs were stably expressed in MDA-MB-231 cells, and ASRPS fusion protein levels were determined by Western blot analysis with anti-FLAG antibody (L), immunostained using anti-FLAG (M) and ASRPS antibodies (N; scale bars, 10 μm). Representative of three (B–N) experiments, respectively. Data are presented as the mean \pm SEM (B and C) or \pm SD (D); ns, not significant by Student's *t* test. KI, knockin; EV, empty vector.

fractions: nonribosome (mRNPs without any ribosome), 40S-80S (mRNPs associated with ribosome but not being translated), and polysome (mRNPs being actively translated). The quantification of ASRPS RNA was determined via qRT-PCR in each fraction (Fig. S1 K). We showed that ASRPS RNA was enriched in the polysome fraction in the MDA-MB-231 cell. Using a Cy3-labeled in situ hybridization probe for *LINC00908* and a FITC-labeled anti-ASRPS antibody, we detected both *LINC00908* and ASRPS in the same tumor (Fig. S1 L) or adjacent normal tissues (Fig. S1 M), and both were highly expressed in the adjacent normal tissue. Furthermore, we generated rabbit polyclonal antibody against ASRPS, and both ASRPS-GFP and ASRPS-FLAG fusion proteins were detected (Fig. 1, J, L, and N). When *LINC00908* was silenced by shRNA in MDA-MB-231 and Hs578T cells (Fig. S2 A), the amount of ASRPS detected by ASRPS antibody was significantly lower (Fig. S2, B and C), which further confirmed the specificity of ASRPS antibody.

The presence of ASRPS protein was detected in MCF7 and MDA-MB-231 cell lines by immunofluorescence assay (Fig. 2 A). ASRPS protein was also detected in TNBC and non-TNBC cell lines by Western blot analysis, and ASRPS expression was significantly lower in TNBC than in non-TNBC cell lines (Fig. 2 B). To confirm that ASRPS was translated from *LINC00908* but not processed from other longer peptides, we showed that ASRPS protein was not detected when anti-*LINC00908*-ORF translation-blocking antisense oligo was transfected (Fig. 2 C).

Down-regulation of ASRPS promoted tumor growth in TNBC

To determine whether ASRPS had a function in TNBC progression, we knocked out ASRPS in a mouse xenograft TNBC model. The tumor volume was significantly higher when ASRPS was knocked out in TNBC cells (Fig. 2 D). To determine whether *LINC00908* had a function in TNBC progression besides ASRPS, we knocked down *LINC00908* alone or in combination with ASRPS. We showed that *LINC00908* knockdown alone significantly promoted tumor growth, but did not further augment tumor growth in ASRPS KO TNBC cells (Fig. 2, E and F). Finally, we showed that reintroducing either full-length *LINC00908* or ASRPS into ASRPS-KO TNBC cells could reverse tumor growth (Fig. 2 G). These results suggested that *LINC00908* inhibited TNBC tumor growth mainly through ASRPS.

Low expression of ASRPS was associated with poor survival in TNBC patients

We next determined the expression of ASRPS in matched fresh primary BC and nontumorous tissues by Western blot analysis. ASRPS was down-regulated in TNBC tissues compared with matched nontumorous tissues; however, such down-regulation was not observed in non-TNBC tissues (Fig. 2 H).

To determine whether down-regulation of ASRPS expression was associated with OS among TNBC patients, we first stratified TNBC patients into two different groups: patients with high ASRPS expression (relative expression level greater than median expression level); and patients with low ASRPS expression (relative expression level less than or equal to median expression level). Using the log-rank test and Kaplan–Meier survival curves, we showed that patients with low ASRPS expression had significantly lower OS than patients with high ASRPS expression in both the discovery set (Suzhou cohort, 112 patients; log rank $P = 0.018$, hazard rate = 2.579) and the validation set (Guangzhou cohort, 105 patients; log rank $P = 0.025$, hazard rate = 2.465; Fig. 2, I and J).

ER α directly regulated *LINC00908* transcription

To investigate the underlying mechanism of differential expression of *LINC00908* in TNBC, we constructed luciferase reporter (pGL3-*LINC00908*) using the promoter region of *LINC00908* (C1–C4; Fig. 3 A). Because ER α was down-regulated in TNBC cells compared with non-TNBC cells, we tested the hypothesis that ER α could directly regulate *LINC00908* transcription. We showed that *LINC00908* was significantly reduced in ER $^-$ BC tissues when compared with ER $^+$ BC tissues in TCGA database (Fig. 3 B). Further, we showed that ASRPS polypeptide was significantly down-regulated in ER α^- BC tumor tissues (Fig. 3 C). Next, we knocked down ER α in non-TNBC cell lines and overexpressed ER α in TNBC cell lines (Fig. S3, A and C). Luciferase assay indicated that ER α knockdown in non-TNBC cell lines significantly reduced transcription of *LINC00908*, whereas ER α overexpression (OE) increased transcription of *LINC00908* in TNBC cell lines (Fig. 3, D and E). We also detected the expression level of ASRPS by Western blot (Fig. S3, B and D). This was consistent with the positive correlation between *LINC00908* and ER α expression in BC tissues (Fig. 3, F and G).

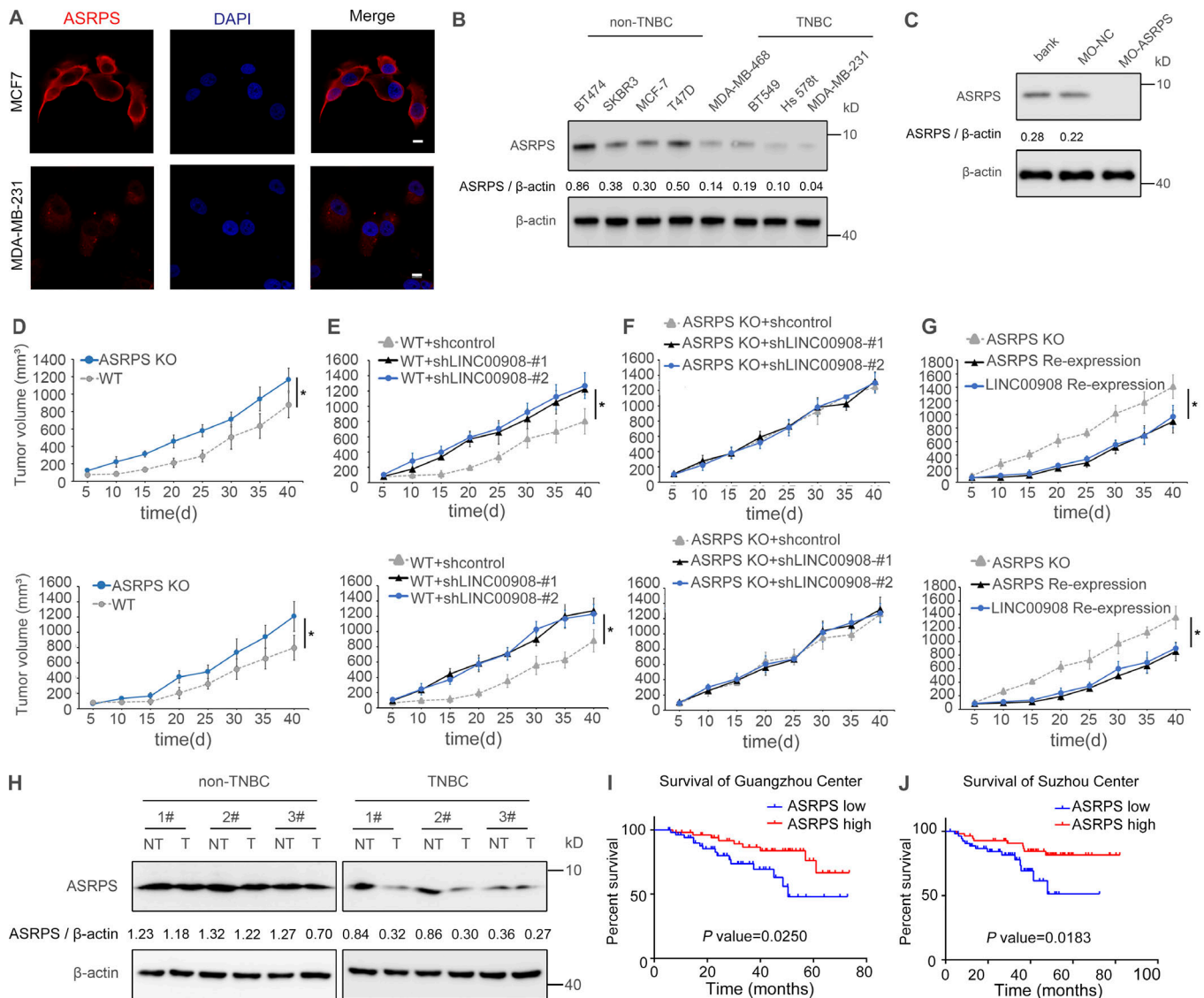


Figure 2. ASRPS was expressed endogenously, down-regulated in TNBC, and associated with poor prognosis in TNBC patients. (A) ASRPS polypeptide was detected in MCF7 and MDA-MB-231 cells by immunofluorescence staining using anti-ASRPS antibody (scale bars, 10 μ m). **(B)** ASRPS polypeptide was detected in various TNBC and non-TNBC cell lines by Western blot analysis using anti-ASRPS antibody. **(C)** *LINC00908* translation-blocking antisense oligo (MO-ASRPS) abolished ASRPS translation in MDA-MB-231 cells. **(D)** ASRPS KO increased tumor growth in mouse xenograft BC model ($n = 5$). **(E)** *LINC00908* knockdown increased tumor growth in mouse xenograft BC model ($n = 5$). **(F)** *LINC00908* knockdown in ASRPS KO cells did not change tumor growth in mouse xenograft BC model ($n = 5$). **(G)** Reintroducing either ASRPS or *LINC00908* in ASRPS KO cells suppressed tumor growth in mouse xenograft BC model ($n = 5$). **(H)** Detection of ASRPS polypeptide in matched non-TNBC (T) and adjacent normal (NT) tissues, and matched TNBC (T) and adjacent normal (NT) tissues. **(I)** Kaplan-Meier OS curves for TNBC patients with high or low ASRPS expression in Guangzhou cohort (105, validation set). **(J)** Kaplan-Meier OS curves for TNBC patients with high or low ASRPS expression in Suzhou cohort (112, discovery set). Representative of three (A–J) experiments, respectively. Data are presented as the mean \pm SD. *, $P < 0.05$ by Student's t test.

Next, we performed the serial deletion experiment to narrow down the promoter region responsible for ER α -regulated *LINC00908* transcription. Luciferase activity was significantly higher in MCF7 cells than in MDA-MB-231 cells as long as the C2 region of the promoter was present (Fig. 3 H). Three binding elements of ER α were identified by PROMO in the C2 promoter region of *LINC00908* (Fig. 3 I). To determine which binding element was required for ER α -mediated *LINC00908* expression, the three predicted ER α binding elements were individually deleted. The deletion experiment indicated that the regulation of ER α is lost in MCF7 when all three elements were deleted

together (Fig. 3 J). To further confirm that C2 region was necessary for ER α -mediated *LINC00908* expression, we performed chromatin immunoprecipitation (ChIP) using anti-ER α antibody followed by analysis of the C1–C4 region by qPCR in TNBC and non-TNBC cell lines. We showed that ER α was bound to the –1,500 to –1,000 region of *LINC00908* promoter in the MCF7 cell line (Fig. 3 K). Luciferase analysis showed that deletion of the three ER α binding elements had no effect on *LINC00908* expression in TNBC cell lines, but significantly reduced *LINC00908* expression in non-TNBC cell lines (Fig. 3, L and M). This was consistent with the observation that the expression of

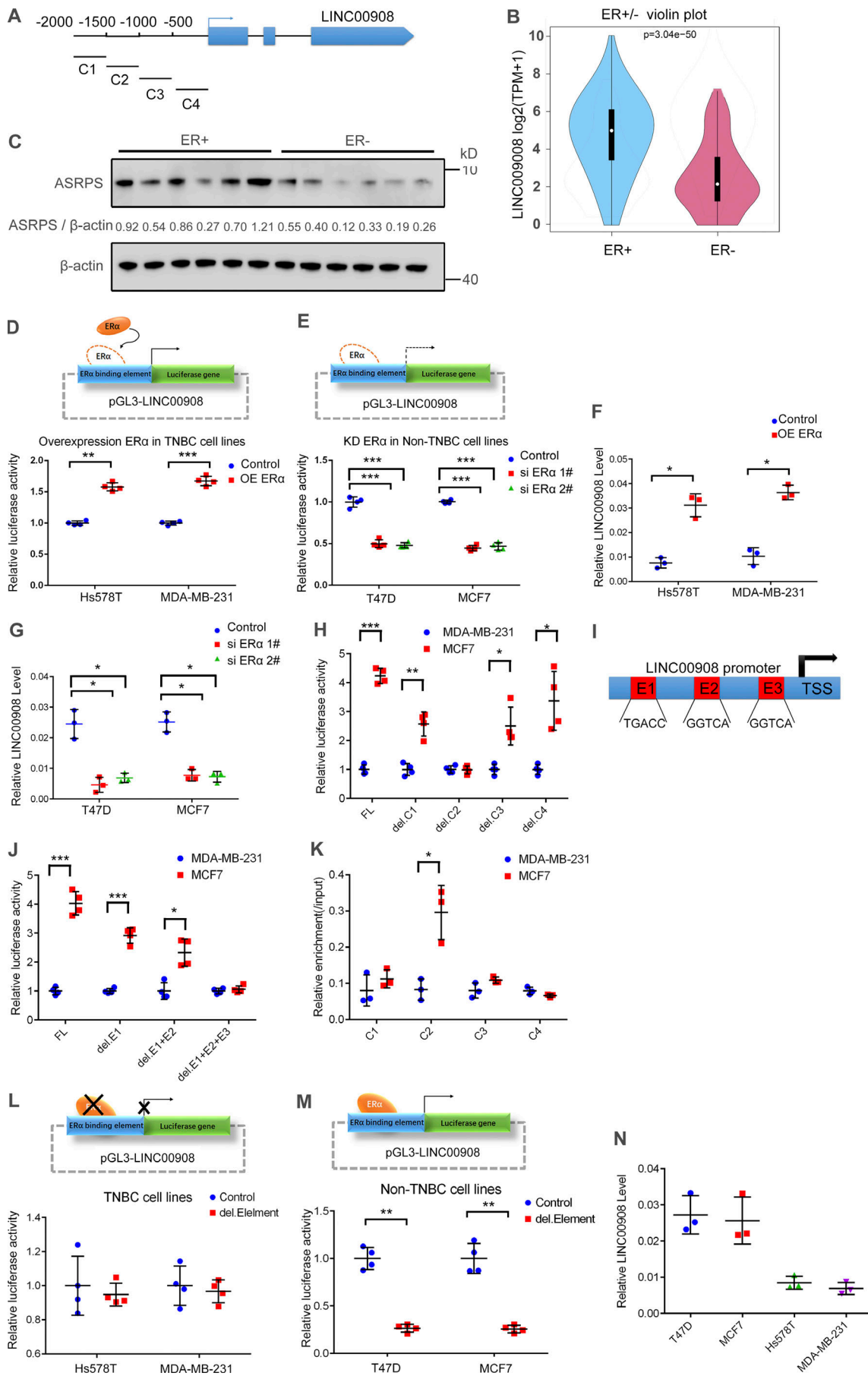


Figure 3. ERα directly regulated *LINC00908* transcription. (A) The upstream 2,000 bp (C1–C4) of the promoter region of *LINC00908*. (B) The expression of *LINC00908* in ERα-positive and ERα-negative BC was analyzed in TCGA database (ERα⁺, *n* = 875; ERα⁻, *n* = 247). (C) The expression of ASRPS in ERα-positive and ERα-negative BC tissues. (D) OE of ERα increased *LINC00908* promoter luciferase activity in TNBC cell lines (Hs578T and MDA-MB-231; *n* = 4). (E) ERα knockdown, transfecting ERα-targeting siRNAs (siERα), abolished *LINC00908* promoter luciferase activity in non-TNBC cell lines (T47D and MCF7; *n* = 4). (F) OE of ERα increased *LINC00908* expression in TNBC cell lines (Hs578T and MDA-MB-231; *n* = 3). (G) Knock-down ERα reduced *LINC00908* expression in non-TNBC cell lines (T47D and MCF7; *n* = 3). (H) Deletion (del.) of C2 fragment (–1,500 to –1,000) in the *LINC00908* promoter region completely abolished *LINC00908* promoter luciferase activity in MCF7 cell line (*n* = 4). (I) The C2 fragment (–1,500 to –1,000) in the *LINC00908* promoter region contained three potential ERα responsive elements (E1, E2, and E3). (J) Deletion three ERα responsive elements (E1, E2, and E3) abolished *LINC00908* promoter luciferase activity in MCF7 cell line (*n* = 4). (K) ERα occupancy measured by ChIP at the C2 fragment of *LINC00908* promoter was enriched in MCF7 cells (*n* = 3). (L) Deletion of three ERα responsive elements had no effect on *LINC00908* promoter luciferase activity in TNBC cell lines (Hs578T and MDA-MB-231). (M) Deletion of three ERα responsive elements abolished *LINC00908* promoter luciferase activity in non-TNBC cell lines (T47D and MCF7; *n* = 4). (N) Relative expression level of *LINC00908* in non-TNBC and TNBC cell lines (*n* = 3). Representative of three (C–N) experiments, respectively. Data are presented as the mean ± SD. *, *P* < 0.05; **, *P* < 0.01; ***, *P* < 0.001 by Student's *t* test. FL, full length.

LINC00908 was significantly higher in non-TNBC cell lines than in TNBC cell lines (Fig. 3 N). Moreover, we showed that 17 β-estradiol (E2) treatment promoted ASRPS in MCF7 cells, but not in MDA-MB-231 cells (Fig. S3 E).

ASRPS interacted with STAT3

Next, we performed an immunoprecipitation experiment in order to identify ASRPS-interacting proteins. We first transfected the ASRPS-FLAG construct into MDA-MB-231 and Hs578T cell lines. 48 h after transfection, the cell lysates were used to perform protein immunoprecipitation using the anti-FLAG antibody. Subsequently, mass spectrometry was used to identify coprecipitated proteins. Potential contaminated proteins were filtered out using the CRAPome database. We identified three candidate proteins that might bind to ASRPS, and we showed that only STAT3 was precipitated by anti-FLAG antibody (Fig. 4, A and B). We showed that the presence of RNase A did not abolish the interaction between ASRPS and STAT3, suggesting that the interaction between ASRPS and STAT3 was not mediated by RNA (Fig. 4 C). We next cotransfected ASRPS-FLAG and STAT3-HA into 293T, MCF7, and T47D cell lines. Both coimmunoprecipitation (coIP) and Western blot analysis showed that ASRPS directly interacted with STAT3 (Fig. 4 D). We further showed that endogenous ASRPS and STAT3 were present in the same protein complex (Fig. 4 E). We used mass spectrometry from coIP with STAT3 antibody in MCF7 to verify the presence of ASRPS (Fig. S3 F). We next determined which conserved domain of STAT3 was responsible for the interaction with ASRPS (Fig. 4 F). Serial deletion analysis of STAT3 indicated that the coiled-coil domain (CCD) of STAT3 was essential for the interaction with ASRPS (Fig. 4, G and H).

ASRPS inhibited STAT3 phosphorylation

Because phosphorylation at tyrosine 705 was essential for STAT3 activation (Yan et al., 2015), we determined whether ASRPS affected STAT3 phosphorylation. Because ASRPS expression was lower in TNBC cells than in non-TNBC cells, we overexpressed ASRPS in the TNBC cell line (MDA-MB-231) and knocked out ASRPS in the non-TNBC cell line (MCF7; Fig. S3 G). We showed that knocking out ASRPS in MCF7 cells increased IL-6-induced STAT3 phosphorylation. In MDA-MB-231 cells, STAT3 was phosphorylated even in the absence of IL-6 due to low expression of ASRPS, and ASRPS OE in MDA-MB-231 cells

reduced STAT3 phosphorylation in the absence of IL-6 (Fig. 4 I). To investigate how ASRPS influenced STAT3 phosphorylation, we determined whether ASRPS directly interfered the interaction of JAK2 (the canonical kinase of STAT3) and STAT3 (Banerjee and Resat, 2016). coIP analysis indicated that both ASRPS and JAK2 coprecipitated with STAT3, and the amount of JAK2 associated with STAT3 was inversely correlated with the amount of ASRPS present in the complex (Fig. 4, J and K). To determine whether ASRPS also affected STAT3 transcriptional activity, we constructed a luciferase reporter using the STAT3-specific binding acute phase response element (APRE). We showed that IL-6-mediated STAT3 transcriptional activity was enhanced by down-regulation of ASRPS in MCF7 cells (Fig. 4 L). In MDA-MB-231 cells, both IL-6-dependent and IL-6-independent STAT3 transcriptional activities were reduced by OE of ASRPS (Fig. 4 M). Immunohistochemistry analysis showed that ASRPS expression level was negatively correlated with p-STAT3 in TNBC tissue samples (Fig. 4 N). Our data indicated that ASRPS inhibited STAT3 phosphorylation as well as its transcriptional activity.

Generation of ASRPS KO BC cell lines using CRISPR/Cas9 system

To further explore the role of ASRPS polypeptide in TNBC progression, we deleted ASRPS in two TNBC cell lines (Hs578T and MDA-MB-231) using the CRISPR/Cas9-mediated homologous recombination technique (Fig. S3, G–J). Two independent KO cell lines (Hs578TKO and MDA-MB-231KO) were generated. Sequence analysis revealed that both cell lines contained mutations at the ATG codon that prevented the translation of ASRPS (Fig. S3 G). We showed that in ASRPS KO cell lines, translation of ASRPS was decreased by polysome profiling and Western blot analysis, but transcription of *LINC00908* was not affected by qRT-PCR analysis (Fig. S3, H–J).

ASRPS regulated the STAT3/VEGF signaling pathway

Previous reports indicated that the VEGF promoter contained the STAT3 binding site and STAT3 activation directly regulated VEGF expression (Niu et al., 2002; Wei et al., 2003). We determined whether ASRPS could affect VEGF expression through regulating STAT3 activation. We detected the canonical STAT3-binding motif in the JASPAR Database (Fig. 5 A). We used ChIP assay to measure STAT3 binding to the VEGF promoter and the

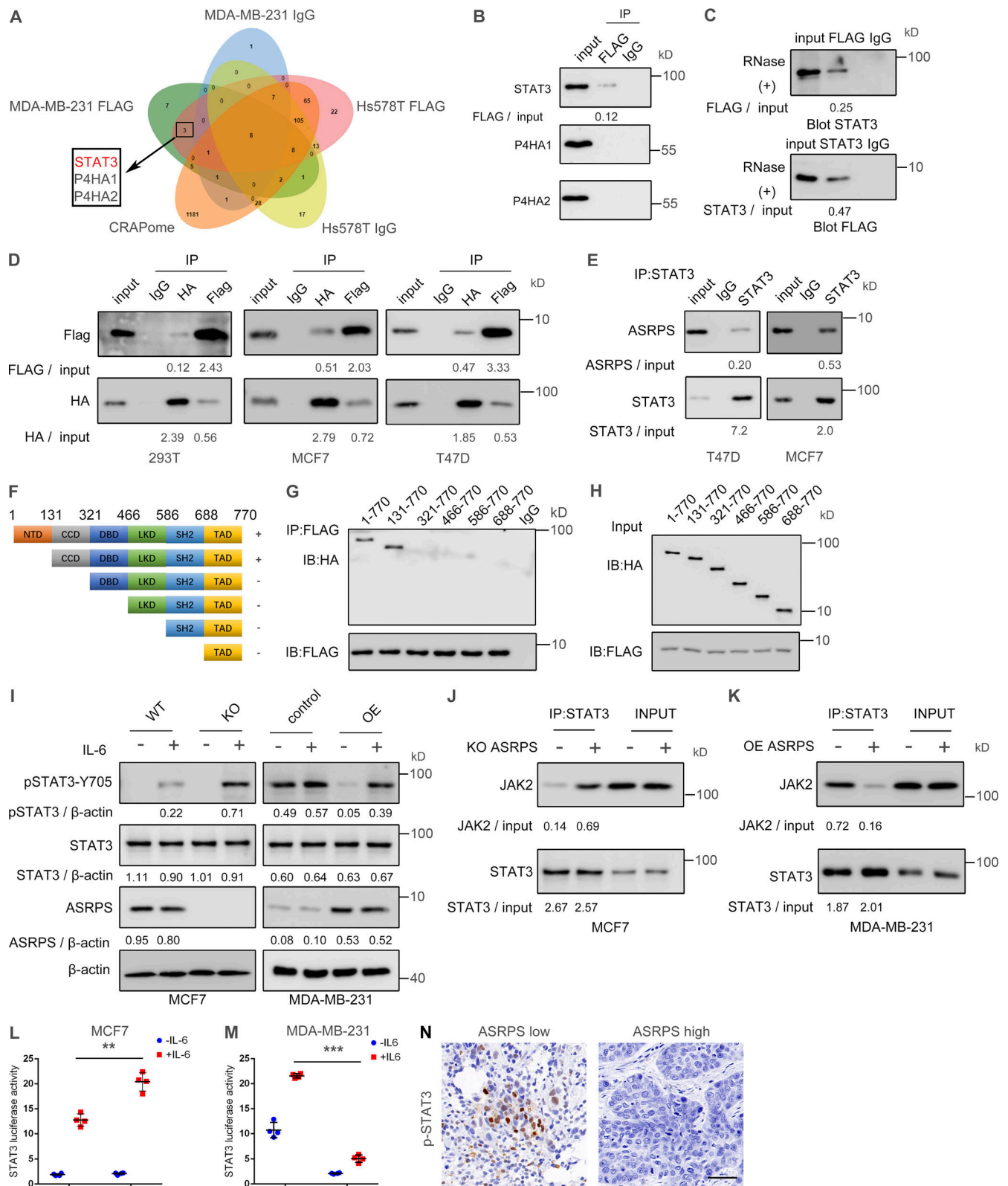


Figure 4. ASRPS interacted with STAT3 and inhibited its phosphorylation. (A) The Venn diagram demonstrated coIP of STAT3, P4HA1, and P4HA2 with ASRPS identified by mass spectrometry analysis. **(B)** STAT3 protein was coimmunoprecipitated with ASRPS-FLAG fusion protein using anti-FLAG antibody in MDA-MB-231 cell lines. **(C)** RNase A treatment did not affect coIP of ASRPS and STAT3 complex. **(D)** ASRPS-FLAG and STAT3-HA fusion proteins were coimmunoprecipitated when both expressed in 293T, MCF7, and T47D cell lines. **(E)** Endogenous ASRPS and STAT3 were coimmunoprecipitated in T47D and MCF7 cell lines. **(F)** STAT3 contains six structural domains (NTD, CCD, DBD, LKD, SH2, and TAD). **(G and H)** Serial deletion analysis of STAT3 to identify ASRPS interacting domain. Truncated STAT3-HA and ASRPS-FLAG were cotransfected in 293T cells. ASRPS was immunoprecipitated with anti-FLAG antibody.

Coimmunoprecipitated truncated STAT3 protein was detected by anti-HA antibody (G). Total input truncated STAT3 protein was detected by anti-HA antibody (H). **(I)** In MCF-7 cells, ASRPS KO increased STAT3 phosphorylation at Y705 after IL-6 treatment. In MDA-MB-231 cells, ASRPS OE reduced STAT3 phosphorylation at Y705 in the absence of IL-6 treatment. **(J)** In MCF-7 cells, ASRPS KO increased the interaction between STAT3 and its kinase JAK2. **(K)** In MDA-MB-231 cells, ASRPS OE decreased the interaction between STAT3 and its kinase JAK2. **(L)** In MCF-7 cells, ASRPS KO increased STAT3 transcriptional activity by APRE-luciferase and Renilla luciferase reporters ($n = 4$). **(M)** In MDA-MB-231 cells, ASRPS OE reduced STAT3 transcriptional activity by APRE-luciferase and Renilla luciferase reporters ($n = 4$). **(N)** p-STAT3 was detected in TNBC tissues of low ASRPS expression by immunohistochemistry analysis (scale bars, 10 μm). Representative of three (A–N) experiments, respectively. Data are presented as the mean \pm SD. **, $P < 0.01$; ***, $P < 0.001$ by Student's t test. IP, immunoprecipitation; IB, immunoblot.

VEGF promoter luciferase assay to measure its expression in TNBC cell lines (Fig. 5, B and C). We showed that ASRPS OE led to reduced binding of STAT3 to the VEGF promoter and reduced VEGF promoter activity, while ASRPS KO enhanced binding of STAT3 to the VEGF promoter and increased VEGF promoter activity. In vivo, we showed that ASRPS expression level in TNBC cell lines negatively correlated with VEGF expression (Fig. 5 D), and secreted VEGF level in the culture medium measured by ELISA was also negatively correlated with ASRPS expression level in TNBC cell lines (Fig. 5 E). However, when cells were treated with STAT3 inhibitor Stattic, VEGF expression was reduced regardless of ASRPS expression level, which correlated with a reduced level of phosphorylated STAT3 (Fig. 5, F and G). These results suggested that ASRPS regulated VEGF expression via STAT3 phosphorylation.

ASRPS repressed tumor angiogenesis

Because VEGF is a key player in angiogenesis and it also regulates proliferation and migration of vascular endothelial cells and tumor cells, we determined the effect of ASRPS expression on angiogenesis and migration of vascular endothelial cells. HUVECs were incubated with conditional medium collected from TNBC cells expressing variable amount of ASRPS, and the capillary tube formation, migration, and wound healing of the HUVECs were measured. ASRPS OE in TNBC significantly reduced the amount of capillary tubes formation by HUVECs, as well as migration and wound-healing ability. On the contrary, ASRPS down-regulation in TNBC significantly increased the tube formation, migration, and wound-healing ability (Fig. 6, A–C; and Fig. S4, A–C). Using an in vitro three-dimensional spheroid-based angiogenesis assay, ASRPS OE in TNBC reduced sprout generation in HUVECs, while ASRPS down-regulation in TNBC significantly induced sprout growth (Fig. 6 D and Fig. S4D). The F-actin staining indicated that the cytoskeleton arranged regularly in ASRPS knock-down cells while the cytoskeleton was in a nest shape and arranged irregularly in ASRPS OE cells, so we counted the percentage of the cells whose cytoskeleton were neatly arranged across the cell's length (Fig. 6 E and Fig. S4 E). Electron microscopy analysis indicated that HUVEC junctions were tighter when incubated with medium collected from MDA-MB-231-overexpressing ASRPS (Fig. 6 F). In vivo Matrigel plug angiogenesis assay indicated that ASRPS expression level in TNBC cells inversely correlated with blood vessel formation (Fig. 6 G). Using a mouse xenograft model, we showed that ASRPS expression level negatively correlated with vascular endothelial cell marker CD31 expression and generation of microvessels (Fig. 6 H and Fig. S4 F). Similarly,

ASRPS expression level in human TNBC tissues negatively correlated with CD31 expression level (Fig. 6 I).

We also determined the effect of *LINC00908* on angiogenesis. Using a pull-down assay, we showed that *LINC00908* did not directly interact with ASRPS (Fig. S5 A). When we overexpressed *LINC00908-mut* (in which the start codon ATG was mutated to ATT so no ASRPS was translated) in WT MDA-MB-231 and ASRPS OE MDA-MB-231 cells (Fig. S5 B), *LINC00908-mut* did not improve the level of phosphorylated STAT3 (Fig. S5 C). When these cells were injected subcutaneously into the hind flanks of the mice, there was no significant difference in angiogenesis in the tumor. Finally, *LINC00908-mut* OE did not reverse the effect of ASRPS OE (Fig. S5, D and E).

STAT3C expression fully reversed the effect of ASRPS OE

Since STAT3C has been reported to spontaneously dimerize through disulfide bonds (Bromberg et al., 1999), we determined whether overexpressed STAT3C in TNBC cells could reverse tumor angiogenesis suppressed by ASRPS OE. STAT3C indeed inversely promotes the expression of VEGF suppressed by ASRPS (Fig. 7, A–C). We showed that OE STAT3C could increase tube formation, migration, and wound-healing ability (Fig. 7, D–F; and Fig. S4, G–I). STAT3C expression also promoted sprout generation (Fig. 7 G and Fig. S4 J) and cytoskeleton organization (Fig. 7 H and Fig. S4 K) in HUVECs. STAT3C expression also promoted angiogenesis in the Matrigel plug angiogenesis assay (Fig. 7 I). In the mouse xenograft model, the CD31 immunofluorescence staining of tumor indicated that STAT3C expression increased generation of microvessels (Fig. 7 J and Fig. S4 L). Based on the above results, we concluded that STAT3C OE fully reversed the effect of ASRPS OE.

ASRPS inhibited BC angiogenesis in MMTV-PyMT mouse mammary tumor model

To further confirm the role of ASRPS in BC angiogenesis, we generated a mouse model by introducing ASRPS into *MMTV-PyMT* mice to generate *MMTV-PyMT; ASRPS^{+/+}* mice. Immunostaining with anti-CD31 indicated that the recruitment of blood vessels was significantly decreased in *MMTV-PyMT; ASRPS^{+/+}* mouse tumor (Fig. 8 A). We also showed that direct injection of exogenous ASRPS into the mammary pad of *MMTV-PyMT* mice significantly reduced angiogenesis in the primary tumor (Fig. 8 B). We concluded that ASRPS inhibited tumor angiogenesis in the *MMTV-PyMT* mouse mammary tumor model.

ASRPS is a potential antitumor peptide

Because ASRPS could inhibit angiogenesis in mouse mammary tumor models, we determined whether ASRPS had antitumor activity. In the TNBC mouse xenograft model, intratumoral

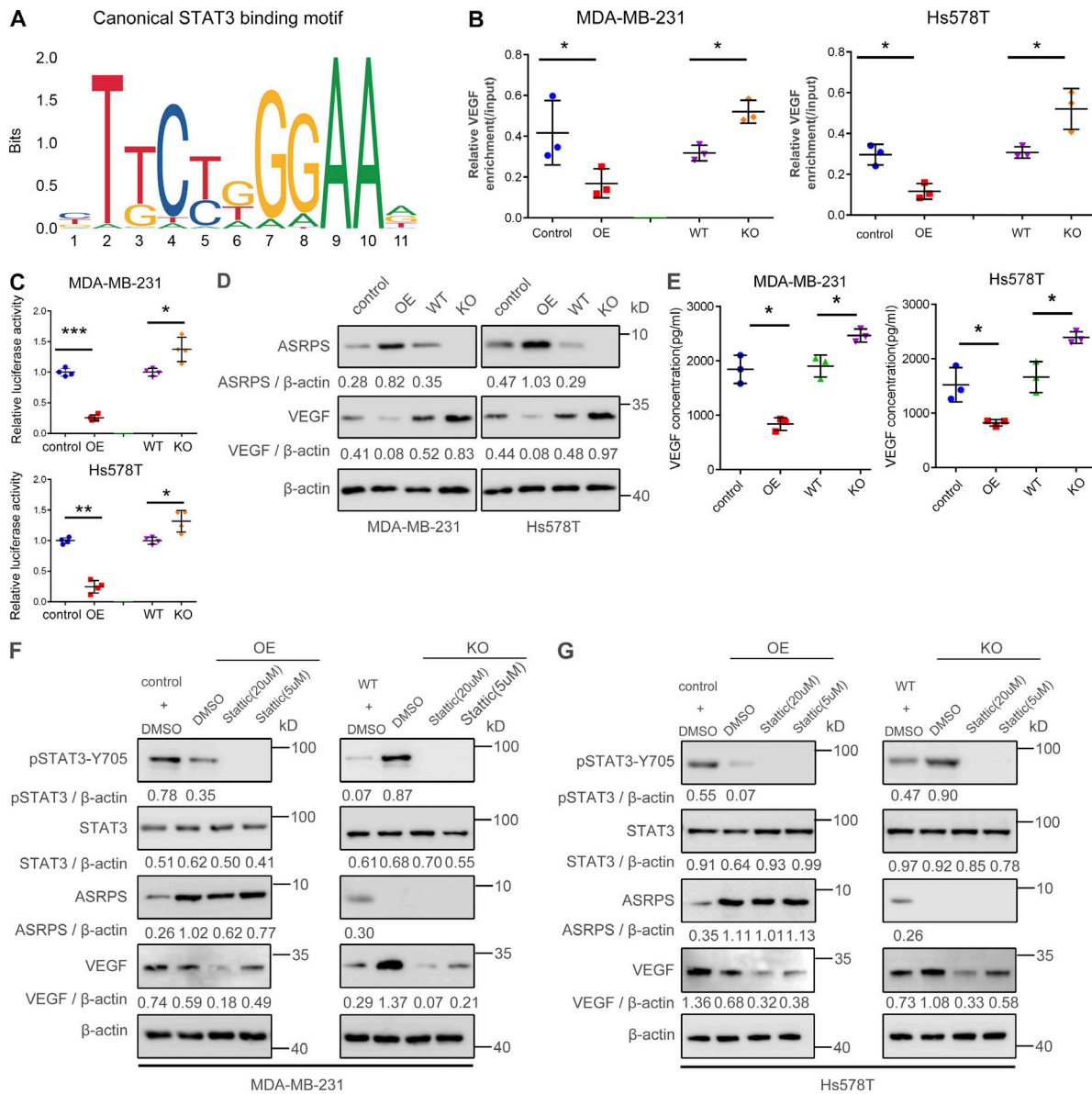


Figure 5. ASRPS regulated the STAT3/VEGF signaling pathway. (A) Canonical STAT3-binding motif (JASPAR Database). **(B)** Enrichment of STAT3 protein at VEGF locus by ChIP assays in TNBC cell lines (MDA-MB-231 and Hs578T) with ASRPS OE or ASRPS KO ($n = 3$). **(C)** VEGF promoter luciferase reporter activity was reduced in TNBC cell lines (MDA-MB-231 and Hs578T) with ASRPS OE but increased with ASRPS KO ($n = 4$). **(D)** VEGF protein level detected by Western blot analysis was reduced in TNBC cell lines (MDA-MB-231 and Hs578T) with ASRPS OE but increased with ASRPS KO. **(E)** The secreted VEGF protein level detected by ELISA was reduced in TNBC cell lines (MDA-MB-231 and Hs578T) with ASRPS OE but increased with ASRPS KO ($n = 3$). **(F and G)** Phosphorylation of STAT3 and VEGF protein expression was completely blocked by Stattic treatments regardless of ASRPS expression level in MDA-MB-231 cells (F) and Hs578T cells (G). Representative of three (B–G) experiments, respectively. Data are presented as the mean \pm SD. *, $P < 0.05$; **, $P < 0.01$; ***, $P < 0.001$ by Student's t test.

injection of ASRPS significantly improved survival (Fig. 8 C). Furthermore, the immunostaining with anti-CD31 of mouse xenograft tumor showed that ASRPS significantly reduced the angiogenesis (Fig. 8 D). These results indicated that ASRPS could improve OS by effectively suppressing tumor angiogenesis.

Discussion

Using the GWIPS-viz database, we identified 26 lncRNAs that were differentially expressed in TNBCs when compared with

adjacent normal tissues, as well as when compared with non-TNBC tissues. TNBC-specific expression of *LINC00908* was regulated by ER α . Both in silico and in vitro analyses indicated that *LINC00908* encoded a polypeptide (ASRPS). ASRPS was down-regulated in TNBC, associated with increased tumor growth and poor OS. We showed that ASRPS was directly bound to STAT3, inhibited phosphorylation of STAT3, down-regulated VEGF expression, and therefore reduced tumor angiogenesis in both BC cell lines and mouse BC models. Finally, we showed that ASRPS is a potent antitumor peptide.

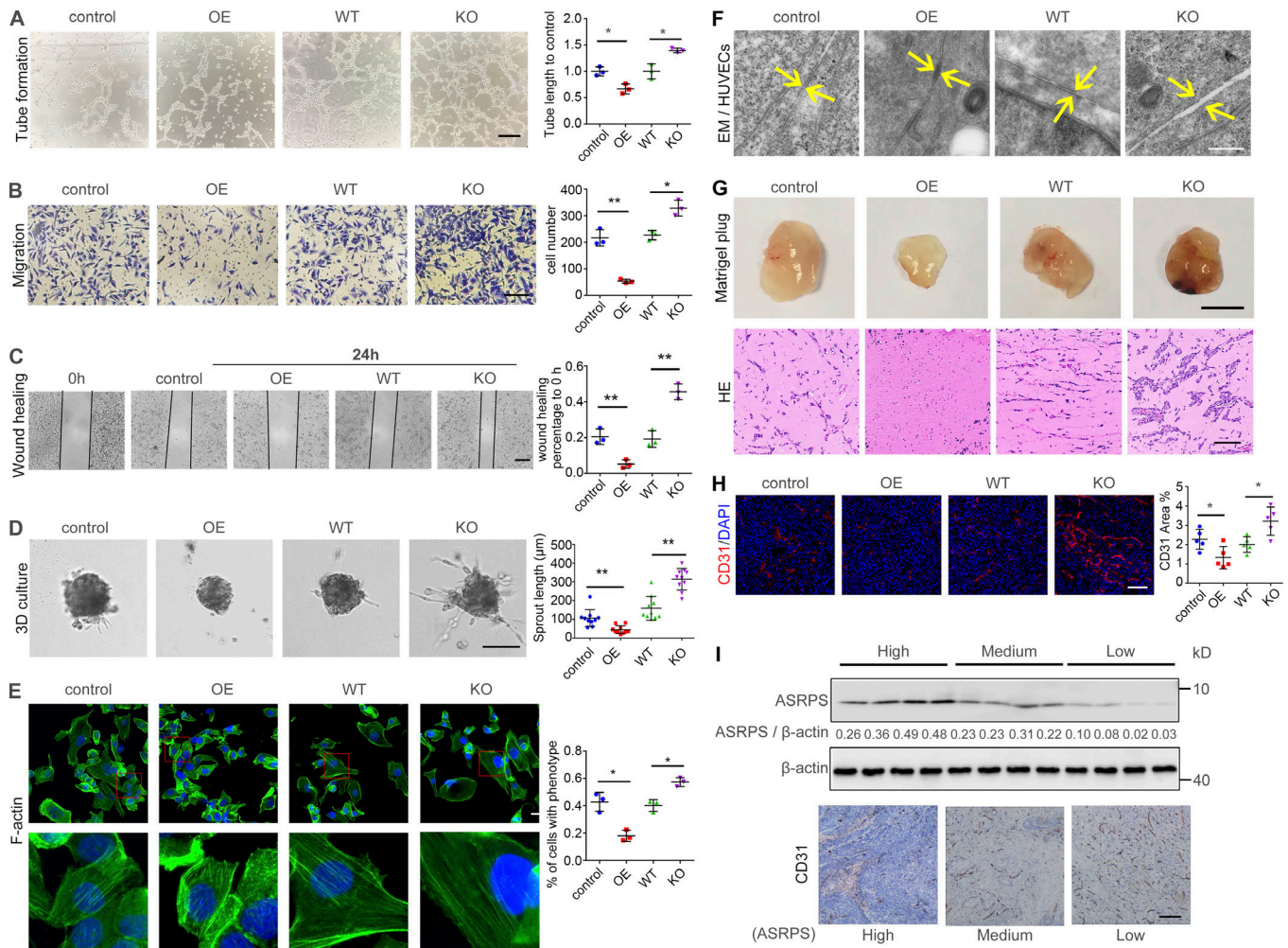


Figure 6. ASRPS repressed tumor angiogenesis. HUVECs were incubating with conditioned medium prepared from MDA-MB-231 cells with ASRPS OE or KO. **(A–F)** Matrigel tube formation (scale bar, 200 µm; $n = 3$; A), transwell migration (scale bar, 50 µm; $n = 3$; B), wound healing migration (scale bars, 200 µm; $n = 3$; C), sprouting assay (scale bars, 200 µm; $n = 10$; D), cytoskeletal reorganization (scale bar, 20 µm; $n = 3$; E) and cell junction of HUVECs observed by electron microscopy. Arrows indicate the cell junction (scale bar, 500 nm; F) of HUVECs. **(G)** Matrigel plugs with HUVECs injected into nude mice subcutaneously. HE stainings were performed on vessel formation within the Matrigel plugs (scale bars, Matrigel plug, 5 mm; HE, 100 µm). **(H)** CD31 expression in mouse BC xenograft model injected with MDA-MB-231 cells with ASRPS OE or ASRPS KO (scale bar, 100 µm; $n = 5$). **(I)** Western blot analysis of ASRPS protein and immunohistochemistry analysis of CD31 protein in TNBC tissues (scale bars, 100 µm). Representative of three (A–I) experiments, respectively. Data are presented as the mean \pm SD. *, $P < 0.05$; **, $P < 0.01$ by Student's t test. HE, hematoxylin-eosin staining; EM, electron microscopy.

Several studies analyzed lncRNA expression profiles in TNBC. Yang et al. (2018) analyzed lncRNA expression profiles between 111 TNBC and 104 noncancerous tissues using RNA sequencing data from TCGA, and identified 1,441 lncRNAs differentially expressed in TNBC, and 109 of them were associated with survival. However, it was unclear whether these differentially expressed lncRNAs were specific to TNBC. Lv et al. (2016) analyzed lncRNA expression levels in three TNBC and three age-matched non-TNBC samples, and identified 880 up-regulated and 784 down-regulated lncRNAs in TNBC. 70 of these lncRNAs were further analyzed in 46 BC tissues and BC cell lines. 38 of them were up-regulated and 32 were down-regulated in TNBC. A panel of four lncRNAs could be used as biomarkers to diagnose TNBC (Lv et al., 2016). Liu et al. (2016) performed transcriptome analysis on 165 TNBC samples and identified various lncRNAs associated with TNBC

subtypes. Koduru et al. (2017) analyzed publicly available small RNA sequencing data derived from 24 TNBC samples and identified 61 differentially expressed lncRNA. 28 were up-regulated and 33 were down-regulated. In the current study, we focused on identifying TNBC-specific lncRNAs with coding potential. Using publicly available sequencing data on TNBC tissues, we first identified lncRNAs that were differentially expressed in TNBC tissues when compared with adjacent normal tissues, then selected those lncRNAs that were not differentially expressed in non-TNBC tissues when compared with normal tissues. We identified one lncRNA, LINC00908, which was differentially expressed in TNBC and encoded a polypeptide, ASRPS. Although polypeptide-encoding lncRNAs have been reported before (Huang et al., 2017), to our knowledge, LINC00908 was the first polypeptide-encoding lncRNA differentially expressed in TNBC.

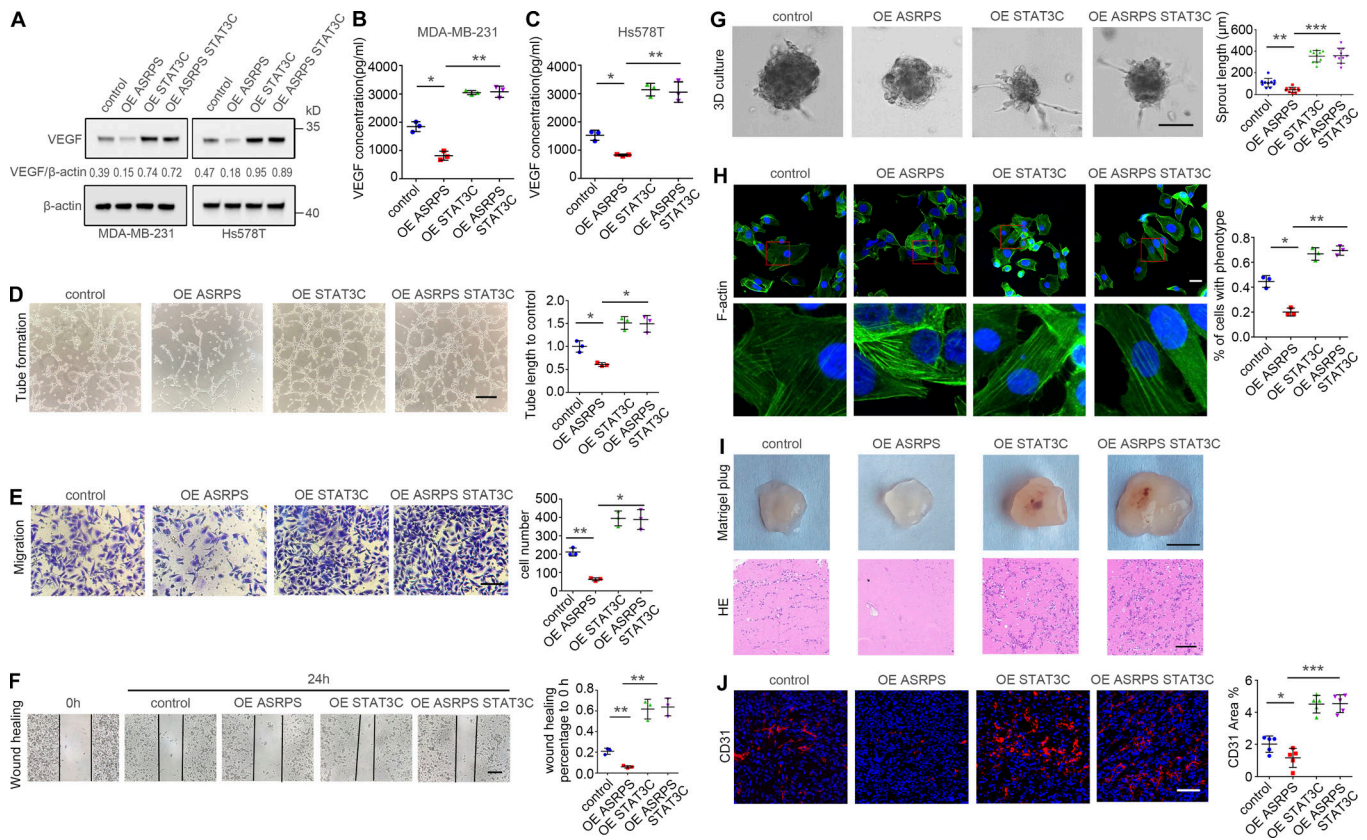


Figure 7. STAT3C expression fully reversed the effect of ASRPS OE. (A) VEGF protein level detected by Western blot analysis. **(B and C)** The secreted VEGF protein level detected by ELISA in TNBC cell lines culture medium ($n = 3$). HUVECs were incubating with conditioned medium prepared from MDA-MB-231 cells with ASRPS OE, STAT3C OE, and ASRPS, STAT3C OE. **(D–H)** Matrigel tube formation (scale bar, 200 μ m; $n = 3$), transwell migration (scale bar, 50 μ m; $n = 3$), wound healing migration (scale bar, 200 μ m; $n = 3$), sprouting assay (scale bar, 200 μ m; $n = 10$), cytoskeletal reorganization (scale bar, 20 μ m; $n = 3$), HE stainings were performed on vessel formation within the Matrigel plugs (scale bars, Matrigel plug, 5 mm; HE, 100 μ m). **(J)** CD31 expression in mouse BC xenograft model injected with MDA-MB-231 cells with ASRPS OE, STAT3C OE and ASRPS, and STAT3C OE (scale bars 50 μ m, $n = 5$). Representative of three (A–J) experiments, respectively. Data are presented as the mean \pm SD. *, $P < 0.05$; **, $P < 0.01$; ***, $P < 0.001$ by Student's t test.

To elucidate the mechanism of TNBC-specific expression of *LINC00908*, we analyzed the *LINC00908* promoter. Using the luciferase reporter assay, we showed that *LINC00908* expression as well as ASRPS was directly regulated by ER α expression. Promoter deletion and ChIP analyses indicated that ER α was directly bound to the -1,500 to -1,000 region in the *LINC00908* promoter. This was consistent with our clinical data that *LINC00908* expression was significantly higher in ER $^+$ BC than ER $^-$ BC. Previous studies have identified ER-regulated lncRNAs in BC. For example, Zhang et al. (2017b) identified 114 ER-regulated lncRNAs in BC by a genome-wide analysis; Li et al. (2018) identified lncRNA *MIAT* overexpressed in ER $^+$ BC; Wang et al. (2019) showed that *LINC00472* was up-regulated by ER α in BC; and Jonsson et al. (2015) showed that *LINC01016* and *LINC00160* were direct transcription targets of ER α . Our study was the first that reported the identification of ER α regulation of lncRNA expression as well as lncRNA-encoded polypeptide.

Our clinical data indicated that ASRPS expression was down-regulated in TNBC, associated with increased tumor growth and poor OS. To elucidate the functional mechanism of ASRPS, we showed that ASRPS was directly bound to STAT3. All STAT

proteins have similar structures, consisting of six conserved domains: a N terminal domain followed by a CCD, a DNA-binding domain, a linker domain, a SH2 domain, and a C terminal trans-activation domain. Our data indicated that the CCD of STAT3 was essential for the interaction with ASRPS. Previous studies indicate that the CCD of STAT3 is essential for auto-phosphorylation (Ma et al., 2003; Zhang et al., 2000), and certain proteins could inhibit STAT3 activation by binding to STAT3 CCD domain (Chang et al., 2018; Mattagajasingh et al., 2012). Even K116, a STAT3 allosteric inhibitor, inhibited STAT3 phosphorylation at Tyr705 by binding to the CCD of STAT3 (Huang et al., 2018a). Using molecular docking, we showed that the ASRPS binding region in the CCD domain overlaps with K116 binding (Fig. S5 F). This suggests that ASRPS could also affect STAT3 phosphorylation through binding to the STAT3 CCD domain. Further, we showed that ASRPS binding to STAT3 inhibited STAT3 phosphorylation, but also inhibited IL-6-induced STAT3 activation. This is consistent with current knowledge on the STAT3 CCD domain: it is not only essential for its activation via SH2 domain-mediated receptor binding and IL-6 induction, but also essential for its activation via phosphorylation (Zhang et al., 2000).

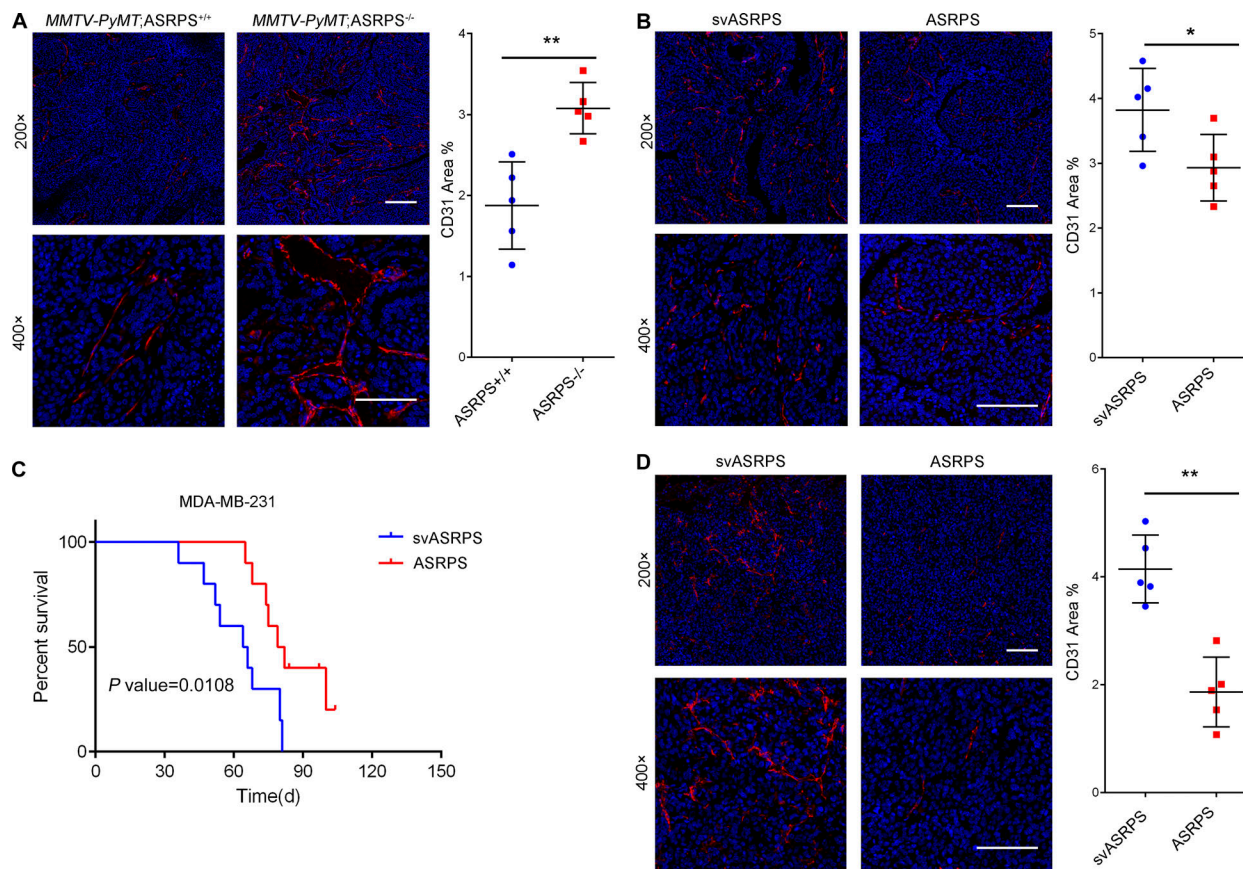


Figure 8. **ASRPS inhibited BC angiogenesis in MMTV-PyMT mouse model.** (A) Tumors from MMTV-PyMT, ASRPS^{+/+} and MMTV-PyMT, ASRPS^{-/-} mice were immunostained with anti-CD31 antibody (scale bars, 100 μ m; $n = 5$). (B) ASRPS protein injection in MMTV-PyMT mice reduced CD31 expression in tumor (scale bars, 100 μ m; $n = 5$). (C) Kaplan–Meier survival curves of mouse BC xenograft model injected with ASRPS ($n = 10$). (D) ASRPS injection in mouse BC xenograft model reduced CD31 expression (scale bars, 100 μ m; $n = 5$). Representative of three (A–D) experiments, respectively. Data are presented as the mean \pm SD. *, $P < 0.05$; **, $P < 0.01$ by Student’s t test. svASRPS, scrambled variant of ASRPS.

Using ASRPS KO BC cell lines as well as mouse BC models, we showed that ASRPS down-regulated VEGF expression and angiogenesis through STAT3 phosphorylation and angiogenesis. In the TNBC mouse model, direct intravenous injection of ASRPS reduced angiogenesis and tumor growth. Only a few studies have identified lncRNAs regulating angiogenesis in BC (Huang et al., 2018b; Zhang et al., 2017a), and no studies have investigated angiogenesis-regulating polypeptide encoded by lncRNA in BC. Our data suggested that ASRPS is a potent antitumor peptide through down-regulating tumor angiogenesis.

It is well known that TNBC is characterized by high cellular proliferation. Consequently, TNBC is associated with increased angiogenesis compared with non-TNBC. Microvascular density is significantly higher in TNBC than in non-TNBC (Ribatti et al., 2016), and VEGF levels are significantly higher in TNBC as well (Bahhnassy et al., 2015). Targeting angiogenesis has been proposed to treat TNBC patients. Our data suggest that ASRPS down-regulated angiogenesis in TNBC and ASRPS is a potent antitumor peptide; therefore, targeting tumor angiogenesis through ASRPS might represent a novel targeted therapy in TNBC.

In summary, we identified an ER α -regulated lncRNA LINC00908, which was down-regulated in TNBC, associated with

increased tumor growth and poor OS. LINC00908 encoded a polypeptide, ASRPS, that regulated angiogenesis in TNBC via the STAT3/VEGF pathway. ASRPS is a potent antitumor peptide. Our results suggest that LINC00908 as well as its encoded ASRPS are potential prognostic markers and therapeutic targets for TNBC.

Materials and methods

Human study subjects

112 pairs of fresh TNBC tissues and their adjacent noncancerous tissues were obtained from patients in eastern China who underwent tylectomies at the Affiliate Hospitals of Soochow University (Suzhou, China). Another 105 pairs of fresh TNBC tissues were collected from patients in southern China at the Cancer Hospitals affiliated with Guangzhou Medical University. These cases were selected based on a clear pathological diagnosis, and the patients had not received preoperative anticancer treatment. This study was approved by the Medical Ethics Committees of Soochow University and the Ethical Committee of Guangzhou Medical University, and written informed consent was obtained from all participants or their appropriate surrogates. The clinical characteristics of the patients are listed in Table S1.

Cell cultures

All cell lines were purchased from Procell Life Science and Technology. These cell lines were all authenticated using short tandem repeat analysis as described in 2012 in the American National Standards Institute standard (ANSI/ATCCASN-0002-2011 Authentication of Human Cell Lines: Standardization of STR Profiling) by the American Type Culture Collection Standards Development Organization and passaged less than 6 mo in this study. DMEM, RPMI-1640, and FBS were purchased from Invitrogen. BT549 and BT474 cells were grown in RPMI-1640 medium supplemented with 10% FBS plus 0.01 mg/ml bovine insulin; MCF7 and T47D cells were grown in MEM supplemented with 10% FBS plus 0.01 mg/ml bovine insulin. MDA-MB-468, MDA-MB-231, and 293T cells were grown in DMEM supplemented with 10% FBS; Hs578T cells were grown in DMEM supplemented with 10% FBS plus 0.01 mg/ml bovine insulin; SKBR3 cells were grown in McCoy's 5A medium supplemented with 10% FBS; and HUVECs were grown in endothelial cell medium (Sciencell, 1001). All cell lines were grown in penicillin/streptomycin-containing medium at 37°C in a humidified atmosphere with 5% CO₂.

Animal breeding and treatments

Nude mice with a BALB/C background (female, 6–8 wk of age) and C57BL/6 WT mice were purchased from Shanghai Laboratory Animal Center at the Chinese Academy of Sciences, Shanghai, China. MMTV-PyMT mice with a C57BL/6 background were obtained from Z. Dong's laboratory at the Institute for Immunology and School of Medicine, Tsinghua University, Beijing, China. The congenic CMV-Cre recombinase mice were constructed from C57BL/6 mice. All animal studies were conducted with the approval of the Soochow University Institutional Animal Care and Use Committee and were performed in accordance with established guidelines.

Hs578T and MDA-MB-231 cell lines were used for various manipulations: (1) ASRPS KO, (2) *LINC00908* knockdown, (3) ASRPS KO/reexpression of ASRPS, (4) ASRPS KO/reexpression of *LINC00908*, and so on. A total of 0.1 ml of cell suspension (1×10^6 /ml) was injected subcutaneously into the hind flanks of the nude mice.

For tumor angiogenesis experiments, PBS or synthetic ASRPS peptide (15 mg/kg) was injected intratumorally in the nude mice when the tumor volume reached ~ 100 mm³. Mice were scheduled for euthanasia when tumor volumes were $\geq 1,000$ mm³. The CD31 immunofluorescence staining of tumors were directly visualized in randomly selected fields. ASRPS (15 mg/kg) was injected into the mammary fat pad of 8-wk-old MMTV-PyMT mice. The CD31 immunofluorescence staining of tumors was directly visualized in randomly selected fields 12 wk after implantation. All WT mice or control mice used in the study are littermates.

Generation of MMTV-PyMT;ASRPS^{+/+} mice

The MMTV-PyMT;ASRPS^{+/+} mice were generated using the gene-targeting construct. A single copy of the ASRPS cDNA was inserted downstream to the STOP cassette (the cassette containing elements designed to terminate both transcription and

translation) through homologous recombination into the ROSA26 (R26) locus, so the exogenous ASRPS cDNA is transcribed under the control of the R26 promoter, allowing a reproducible and stable OE of ASRPS. This gene-targeting construct was electroporated into C57BL/6 mice embryonic stem cells; subsequently the recombinant embryonic stem clones were microinjected to generate chimeric C57BL/6 mice.

To analyze the in vivo consequences of ASRPS OE, conditional knockin animals were crossed with the CMV-Cre strain in order to obtain ASRPS^{+/-} heterozygous mice. ASRPS^{+/+} homozygous animals were generated by intercrossing heterozygous mice. Finally, C57BL/6 ASRPS^{+/+} mice were crossed with C57BL/6 MMTV-PyMT mice to generate MMTV-PyMT;ASRPS^{+/+} on the C57BL/6 background. All mice we used were on a C57BL/6 background.

Data processing and differential expression analysis

The gene expression profile of BC RNA sequencing data and matched clinicopathological information BC patients in this study were downloaded from Genomic Data Commons (<https://gdc.cancer.gov/>). We inspected the gene expression status of ESRI, progesterone receptor, and HER2 of each patient in the clinical data. TNBC patients were defined as patients with negative ESRI and progesterone receptor status, as well as zero HER2 immunohistochemistry level. In total, 113 normal samples, 18 TNBC samples, and 347 non-TNBC samples were selected for the differential expression analysis. DESeq2 was applied to identify the differentially expressed genes between TNBCs and normal samples, and between TNBCs and non-TNBCs. Genes were considered as statistically significantly differentially expressed with a false discovery rate < 0.01 and absolute log₂ fold change > 2.

Prediction of lncRNAs with coding ability

The human lncRNAs sequences were obtained from GENCODE. Small ORFs of lncRNAs were predicted by ORFFinder using the parameters with “-strand plus -ml 30 -s 0.” The predicted ORFs were aligned to the human reference genome version hg38 using Bowtie2 and transformed to BED format by Bedtools. Then the predicted ORFs overlapping with the GWIPS-viz dataset that filtered with data value ≥ 100 were extracted by UCSC Table Browser. Finally, these ORFs were annotated using R package ChIPseeker.

Statistics

All experiments were repeated at least three times unless stated in the figure legends. Two-tailed paired Student's *t* tests were applied for comparison between two groups. Survival curves were obtained using the Kaplan–Meier method and compared using the log-rank test. Statistical analyses were performed using Prism 7 software. The data were presented as the means \pm SD except where stated otherwise. The differences with *, *P* < 0.05, **, *P* < 0.01, or ***, *P* < 0.001 were considered statistically significant.

Real-time qRT-PCR

Trizol total RNA isolation reagent (Invitrogen) was used for extracting total RNA from cells and tissues. cDNA was then generated by reverse transcription of aliquots of RNA using

M-MLV RNase H-Reverse transcription (Comiike) according to the manufacturer's instructions, and the cDNA was used for real-time quantitative PCR using Novostart SYBR qPCR Super Mix Plus (Novoprotein). Primers used for real-time RT-PCR are shown in Table S4.

Northern blot analysis

Northern blot was performed to analyze *LINC00908* transcript using NorthernMax Kit (Invitrogen) according to the manufacturer's instructions. About 10 μ g of RNA from each sample was subjected to formaldehyde gel electrophoresis and transferred to a Biotodyne Nylon membrane (Pall). The PCR primers used to generate the Northern blot probe are listed in Table S4.

Polysome profiling

Polysome profiling was performed to measure the translation of ASRPS. We performed the polysome profiling assay as described before (Gandin et al., 2014). The primers for qRT-PCR are listed in Table S4.

Immunofluorescence staining

A series of ORF-GFP fusion plasmids were transfected into MDA-MB-231 cells, and GFP fluorescence was directly visualized by Nikon Eclipse Ti-U fluorescence microscope. MDA-MB-231 and MCF7 cells were plated on glass coverslips, fixed with 4% paraformaldehyde at room temperature for 15 min, rinsed three times with phosphate-buffered saline Triton (PBSTx; 0.3% Triton X-100), incubated with anti-ASRPS antibody and anti-FLAG antibody overnight at 4°C, washed twice with Tris-buffered saline Triton (TBSTx), and incubated with FITC secondary IgG antibodies (Beyotime) at room temperature for 1 h in the dark. Cell nuclei were stained with DAPI. Fluorescence images were analyzed using Leica SP5 Confocal Microscopes.

Tumor tissues were fixed and frozen in optimum cutting temperature compound (Sakura). Sections of 10- μ m thickness were cut at -20°C. The sections were incubated with CD31 overnight at 4°C. After three rinses with PBST (0.3% Triton X-100), sections were incubated for 1 h at room temperature with Cy3 secondary IgG antibodies in the dark (Beyotime). Cell nuclei were stained with DAPI. Fluorescence images were analyzed using Leica SP5 Confocal Microscopes.

RNA FISH

RNA FISH experiments were performed to detect *LINC00908* RNA in BC cells using the FISH Detection Kit (Ribo) according to the protocol.

Cell nucleus/cytoplasm fraction isolation

Cell nucleus/cytoplasm fraction isolation was performed as previously described (Li et al., 2017). To determine the cellular localization of *LINC00908*, cytosolic and nuclear fractions were collected according to the manufacturer's instructions for the nuclear/cytoplasmic Isolation Kit (Biovision).

ASRPS knockin and KO by CRISPR/Cas9

The guide RNA (gRNA) designed specifically for the ASRPS start codon was cloned into the Cas9/gRNA (puro-GFP) vector

(VK001-02, ViewSolid BioTech), and donor oligo was designed and synthesized. All sequence information is shown in Table S4. The gRNA construct and donor oligo were transfected into cells using Lipofectamine 3000 (Invitrogen), following the manufacturer's instructions. Single-cell clones were selected and evaluated using the T7 endonuclease assay to detect mutants. Next, the constructed clones were selected and sequenced using a 3100 Genetic Analyzer (ABI) to confirm the presence of mutation in the target sequence.

Anti-ASRPS antibody preparation

Peptide synthesis and anti-ASRPS antibody generation were performed as previously described with some modifications (Yu et al., 2017). Briefly, a BSA and OVA-coupled peptide RGGRIWSSDPRSDG-Cys was synthesized, and polyclonal antibodies against the *LINC00908* peptide were obtained from inoculated rabbits. Antibodies were purified using affinity chromatography on columns containing the corresponding peptides.

ChIP assay

ChIP in BC cells was performed using ER α and STAT3 antibodies and the ChIP Assay Kit (Millipore) according to the manufacturer's protocol.

Dual-luciferase reporter assay

The corresponding DNA sequence of *LINC00908* promoter was cloned into the pGL3-basic vector (Promega). The promoter with the ER α element deleted was also cloned into the pGL3-basic vector. The luciferase activities of the reporters were measured using the Dual Luciferase Reporter Assay System (Promega) according to the manufacturer's protocol.

Western blot analysis and coIP

Tissues or cells were lysed with radioimmunoprecipitation assay lysis buffer (Solarbio) with protease inhibitor and phosphatase inhibitor. Western blot analysis was performed as in our previous study (Wu et al., 2015), and the Western results were quantified by ImageJ software (Wu et al., 2015).

For immunoprecipitation, cell lysate (~1.5 mg total protein) was harvested using ice-cold nondenaturing lysis buffer (Thermo Fisher Scientific). coIP assay was performed using the Pierce Co-Immunoprecipitation Kit (Thermo Fisher Scientific) according to the manufacturer's protocol. Briefly, the corresponding antibody was first immobilized for 2 h using Amino-Link Plus coupling resin. The resin was then washed and incubated with cell lysate overnight. After incubation, the resin was again washed and protein eluted using elution buffer. All antibodies used are listed in Table S3.

Lentiviral production and transduction

The full length of ASRPS-FLAG was cloned into the lentiviral expression vector pLVX-IRES-neo (Clontech Laboratories). The shRNAs of *LINC00908* lentivirus vector were obtained from ABM. Using a three-plasmid transient cotransfection method (Lenti-T HT packaging mix, Clontech Laboratories), 293T cells were cotransfected with three vectors. Lentiviruses were

harvested and concentrated. For transduction, MCF7, T47D, MDA-MB-231, and Hs578T cells were infected with the concentrated virus in the presence of polybrene (Sigma-Aldrich). After 48 h of transduction, the cells were stably selected with G418 at 500 µg/ml (GIBCO BRL), and the drug-resistant cell populations were selected for subsequent studies. The lentiviruses and plasmids used in this study are listed in Table S2.

siRNA

siRNAs targeting ERα were synthesized by Genepharma. A nontargeting scrambled siRNA (Dharmacon) was used as a control. The knockdown efficiency and specificity of all siRNAs were validated by qRT-PCR. The siRNAs used in this study are listed in Table S5.

Tube formation assay

Matrigel (10 µl, Corning) was first thawed on ice at 4°C overnight, then loaded into each well of a precooled µ-Slide Angiogenesis plate (Ibidi). The plate was incubated at 37°C for 30 min for hardening. 15,000 HUVECs in 100 µl conditioned cell culture medium were plated onto the precoated Matrigel for 6 h. The resulting capillary-like structures were then photographed with a microscope and counted with ImageJ software.

Migration and wound healing assay

For the cell migration assay, HUVECs (10,000 cells) in serum-free media (200 µl) were plated in the upper chamber (Corning), and the conditioned cell culture medium (prepared from ASRPS OE or KO MDA-MB-231/Hs578T cells) was placed in the lower chamber, and incubated for 48 h at 37°C to allow the cells to migrate to the lower chamber. The cells that had migrated through the membrane were fixed with 4% paraformaldehyde for 30 min, then stained with crystal violet (Invitrogen) for 10 min, imaged, and counted using a microscope.

For the wound healing assay, HUVECs were seeded on cell culture inserts (Ibidi) in 35-mm dishes and coincubated with mitomycin C at 37°C in 5% CO₂ and grown to confluence as a monolayer. Then inserts were removed and the conditioned cell culture medium (prepared from ASRPS OE or KO MDA-MB-231/Hs578T cells) was added. After 12 h, cells were imaged. The gap was analyzed using ImageJ software. Each experiment was repeated in triplicate.

Sprouting assay

Spheroids were generated as described before (Korff and Augustin, 1998). Briefly, spheroids embedded into the collagen gel containing the conditional medium were applied on top of the gel. After culturing for 24 h, spheroid sprouts were evaluated by measuring the cumulative length of all capillary-like sprouts using a microscope. At least 10 randomly selected spheroids per experimental group were analyzed. Sprout length was measured with ImageJ software.

ELISA analysis of VEGF expression

VEGF secreted into the culture medium was measured using a Human VEGF ELISA kit (Bio-Swamp) following the manufacturer's protocol. VEGF concentration was calculated using a standard curve.

Matrigel plug assay

The Matrigel plug assay was performed using an in vivo angiogenesis assay. In brief, the conditioned cell culture medium (prepared from ASRPS OE or KO MDA-MB-231/Hs578T cells) was collected. 400 µl of Matrigel mixed with 300 µl of conditioned medium and 5.0×10^6 HUVECs were injected into the ventral area of 6-wk-old nude mice. After 10 d, the skin of mice was pulled back with scissors to expose intact Matrigel plugs, and plug images were taken.

Online supplemental material

Fig. S1 shows screening of candidate lncRNAs and biological characterization of *LINC00908*. Fig. S2 shows that anti-ASRPS antibody specifically detects the polypeptide ASRPS. Fig. S3 shows silencing and OE of ERα, and mass spectrometry results of ASRPS and ASRPS KO in BC cell lines. Fig. S4 shows ASRPS affected migration, invasion, and angiogenesis in BC cell lines, but STAT3C expression fully reversed the effect of ASRPS OE. Fig. S5 shows *LINC00908* cannot have an effect on angiogenesis or reverse the effect of tumor angiogenesis caused by ASRPS. Table S1 shows primary clinical and histological characteristics of 217 study patients. Table S2 shows virus strains and recombinant DNA used in this study. Table S3 shows antibodies used in this study. Table S4 shows primers and gRNA used in this study. Table S5 shows sequences of siRNAs and shRNAs used in this study.

Acknowledgments

This work was supported by the National Scientific Foundation of China (grants 81772544 and 81972649); the Science Foundation for Distinguished Young Scholars in Jiangsu (BK20160008); a project funded by the Priority Academic Program Development of Jiangsu Higher Education Institutions; National Key R&D Program of China (2016YFC1302100); and the Program for Guangdong Introducing Innovative and Entrepreneurial Teams (2017ZT07S096).

The authors declare no competing financial interests.

Author contributions: Y. Zhou designed the study. Y. Wang, S. Wu, L. Zhang, and X. Zhu performed the experiments. F. Li, J. Deng, B. Guo, S. Zhang, R. Wu, Z. Zhang, K. Wang, and J. Lu helped with investigation and formal analysis.

Submitted: 29 May 2019

Revised: 27 September 2019

Accepted: 31 October 2019

References

- Anderson, D.M., K.M. Anderson, C.L. Chang, C.A. Makarewich, B.R. Nelson, J.R. McAnally, P. Kasaragod, J.M. Shelton, J. Liou, R. Bassel-Duby, and E.N. Olson. 2015. A micropeptide encoded by a putative long noncoding RNA regulates muscle performance. *Cell*. 160:595-606. <https://doi.org/10.1016/j.cell.2015.01.009>
- Bahnassy, A., M. Mohanad, S. Shaarawy, M.F. Ismail, A. El-Bastawisy, A.M. Ashmawy, and A.R. Zekri. 2015. Transforming growth factor-β, insulin-like growth factor I/insulin-like growth factor I receptor and vascular endothelial growth factor-A: prognostic and predictive markers in

- triple-negative and non-triple-negative breast cancer. *Mol. Med. Rep.* 12: 851–864. <https://doi.org/10.3892/mmr.2015.3560>
- Banerjee, K., and H. Resat. 2016. Constitutive activation of STAT3 in breast cancer cells: A review. *Int. J. Cancer.* 138:2570–2578. <https://doi.org/10.1002/ijc.29923>
- Brewster, A.M., M. Chavez-MacGregor, and P. Brown. 2014. Epidemiology, biology, and treatment of triple-negative breast cancer in women of African ancestry. *Lancet Oncol.* 15:e625–e634. [https://doi.org/10.1016/S1470-2045\(14\)70364-X](https://doi.org/10.1016/S1470-2045(14)70364-X)
- Bromberg, J.F., M.H. Wrzeszczynska, G. Devgan, Y. Zhao, R.G. Pestell, C. Albanese, and J.E. Darnell Jr. 1999. Stat3 as an oncogene. *Cell.* 98: 295–303. [https://doi.org/10.1016/S0092-8674\(00\)81959-5](https://doi.org/10.1016/S0092-8674(00)81959-5)
- Chang, R., L. Song, Y. Xu, Y. Wu, C. Dai, X. Wang, X. Sun, Y. Hou, W. Li, X. Zhan, and L. Zhan. 2018. Loss of Wwox drives metastasis in triple-negative breast cancer by JAK2/STAT3 axis. *Nat. Commun.* 9:3486. <https://doi.org/10.1038/s41467-018-05852-8>
- Chen, W., R. Zheng, P.D. Baade, S. Zhang, H. Zeng, F. Bray, A. Jemal, X.Q. Yu, and J. He. 2016. Cancer statistics in China, 2015. *CA Cancer J. Clin.* 66: 115–132. <https://doi.org/10.3322/caac.21338>
- Elias, A.D. 2010. Triple-negative breast cancer: a short review. *Am. J. Clin. Oncol.* 33:637–645. <https://doi.org/10.1097/COC.0b013e3181b8afcf>
- Fang, Y., and M.J. Fullwood. 2016. Roles, Functions, and Mechanisms of Long Non-coding RNAs in Cancer. *Genomics Proteomics Bioinformatics.* 14: 42–54. <https://doi.org/10.1016/j.gpb.2015.09.006>
- Foulkes, W.D., I.E. Smith, and J.S. Reis-Filho. 2010. Triple-negative breast cancer. *N. Engl. J. Med.* 363:1938–1948. <https://doi.org/10.1056/NEJMr1001389>
- Gandin, V., K. Sikström, T. Alain, M. Morita, S. McLaughlan, O. Larsson, and I. Topisirovic. 2014. Polysome fractionation and analysis of mammalian translomes on a genome-wide scale. *J. Vis. Exp.* (87). <https://doi.org/10.3791/51455>
- Huang, J.Z., M. Chen, D. Chen, X.C. Gao, S. Zhu, H. Huang, M. Hu, H. Zhu, and G.R. Yan. 2017. A Peptide Encoded by a Putative lncRNA HOXB-AS3 Suppresses Colon Cancer Growth. *Mol. Cell.* 68:171–184.e6. <https://doi.org/10.1016/j.molcel.2017.09.015>
- Huang, M., K. Song, X. Liu, S. Lu, Q. Shen, R. Wang, J. Gao, Y. Hong, Q. Li, D. Ni, et al. 2018a. AlloFinder: a strategy for allosteric modulator discovery and allosterome analyses. *Nucleic Acids Res.* 46(W1):W451–W458. <https://doi.org/10.1093/nar/gky374>
- Huang, X.J., Y. Xia, G.F. He, L.L. Zheng, Y.P. Cai, Y. Yin, and Q. Wu. 2018b. MALAT1 promotes angiogenesis of breast cancer. *Oncol. Rep.* 40: 2683–2689.
- Ingolia, N.T., L.F. Lareau, and J.S. Weissman. 2011. Ribosome profiling of mouse embryonic stem cells reveals the complexity and dynamics of mammalian proteomes. *Cell.* 147:789–802. <https://doi.org/10.1016/j.cell.2011.10.002>
- Jonsson, P., C. Coarfa, F. Mesmar, T. Raz, K. Rajapakshe, J.F. Thompson, P.H. Gunaratne, and C. Williams. 2015. Single-Molecule Sequencing Reveals Estrogen-Regulated Clinically Relevant lncRNAs in Breast Cancer. *Mol. Endocrinol.* 29:1634–1645. <https://doi.org/10.1210/me.2015-1153>
- Koduru, S.V., A.K. Tiwari, A. Leberfinger, S.W. Hazard, Y.I. Kawasaki, M. Mahajan, and D.J. Ravnic. 2017. A Comprehensive NGS Data Analysis of Differentially Regulated miRNAs, piRNAs, lncRNAs and sn/snoRNAs in Triple Negative Breast Cancer. *J. Cancer.* 8:578–596. <https://doi.org/10.7150/jca.17633>
- Kong, X., W. Liu, and Y. Kong. 2018. Roles and expression profiles of long non-coding RNAs in triple-negative breast cancers. *J. Cell. Mol. Med.* 22: 390–394. <https://doi.org/10.1111/jcmm.13327>
- Korff, T., and H.G. Augustin. 1998. Integration of endothelial cells in multicellular spheroids prevents apoptosis and induces differentiation. *J. Cell Biol.* 143:1341–1352. <https://doi.org/10.1083/jcb.143.5.1341>
- Li, W., H. Li, L. Zhang, M. Hu, F. Li, J. Deng, M. An, S. Wu, R. Ma, J. Lu, and Y. Zhou. 2017. Long non-coding RNA LINC00672 contributes to p53 protein-mediated gene suppression and promotes endometrial cancer chemosensitivity. *J. Biol. Chem.* 292:5801–5813. <https://doi.org/10.1074/jbc.M116.758508>
- Li, Y., B. Jiang, X. Wu, Q. Huang, W. Chen, H. Zhu, X. Qu, L. Xie, X. Ma, and G. Huang. 2018. Long non-coding RNA MIAT is estrogen-responsive and promotes estrogen-induced proliferation in ER-positive breast cancer cells. *Biochem. Biophys. Res. Commun.* 503:45–50. <https://doi.org/10.1016/j.bbrc.2018.05.146>
- Li, F., H. Li, L. Zhang, W. Li, J. Deng, M. An, S. Wu, X. Lu, R. Ma, Y. Wang, et al. 2019. X chromosome-linked long noncoding RNA lnc-XLECI regulates c-Myc-dependent cell growth by collaborating with MBP-1 in endometrial cancer. *Int. J. Cancer.* 145:927–940. <https://doi.org/10.1002/ijc.32166>
- Liu, Y.R., Y.Z. Jiang, X.E. Xu, K.D. Yu, X. Jin, X. Hu, W.J. Zuo, S. Hao, J. Wu, G.Y. Liu, et al. 2016. Comprehensive transcriptome analysis identifies novel molecular subtypes and subtype-specific RNAs of triple-negative breast cancer. *Breast Cancer Res.* 18:33. <https://doi.org/10.1186/s13058-016-0690-8>
- Lv, M., P. Xu, Y. Wu, L. Huang, W. Li, S. Lv, X. Wu, X. Zeng, R. Shen, X. Jia, et al. 2016. LncRNAs as new biomarkers to differentiate triple negative breast cancer from non-triple negative breast cancer. *Oncotarget.* 7: 13047–13059. <https://doi.org/10.18632/oncotarget.7509>
- Ma, J., T. Zhang, V. Novotny-Diermayr, A.L. Tan, and X. Cao. 2003. A novel sequence in the coiled-coil domain of Stat3 essential for its nuclear translocation. *J. Biol. Chem.* 278:29252–29260. <https://doi.org/10.1074/jbc.M304196200>
- Matsumoto, A., A. Pasut, M. Matsumoto, R. Yamashita, J. Fung, E. Monteleone, A. Saghatelian, K.I. Nakayama, J.G. Clohessy, and P.P. Pandolfi. 2017. mTORC1 and muscle regeneration are regulated by the LINC00961-encoded SPAR polypeptide. *Nature.* 541:228–232. <https://doi.org/10.1038/nature21034>
- Mattagajasingh, S.N., X.P. Yang, K. Irani, I. Mattagajasingh, and L.C. Becker. 2012. Activation of Stat3 in endothelial cells following hypoxia-reoxygenation is mediated by Rac1 and protein Kinase C. *Biochim. Biophys. Acta.* 1823:997–1006. <https://doi.org/10.1016/j.bbamcr.2012.02.008>
- Niu, G., K.L. Wright, M. Huang, L. Song, E. Haura, J. Turkson, S. Zhang, T. Wang, D. Sinibaldi, D. Coppola, et al. 2002. Constitutive Stat3 activity up-regulates VEGF expression and tumor angiogenesis. *Oncogene.* 21: 2000–2008. <https://doi.org/10.1038/sj.onc.1205260>
- Peng, Z., J. Wei, X. Lu, H. Zheng, X. Zhong, W. Gao, Y. Chen, and J. Jing. 2016. Treatment and survival patterns of Chinese patients diagnosed with breast cancer between 2005 and 2009 in Southwest China: An observational, population-based cohort study. *Medicine (Baltimore).* 95:e3865. <https://doi.org/10.1097/MD.00000000000003865>
- Polycarpou-Schwarz, M., M. Groß, P. Mestdagh, J. Schott, S.E. Grund, C. Hildenbrand, J. Rom, S. Aulmann, H.P. Sinn, J. Vandesompele, and S. Diederichs. 2018. The cancer-associated microprotein CASIMO1 controls cell proliferation and interacts with squalene epoxidase modulating lipid droplet formation. *Oncogene.* 37:4750–4768. <https://doi.org/10.1038/s41388-018-0281-5>
- Ribatti, D., B. Nico, S. Ruggieri, R. Tamma, G. Simone, and A. Mangia. 2016. Angiogenesis and Antiangiogenesis in Triple-Negative Breast Cancer. *Transl. Oncol.* 9:453–457. <https://doi.org/10.1016/j.tranon.2016.07.002>
- Rodríguez Bautista, R., A. Ortega Gómez, A. Hidalgo Miranda, A. Zentella Dehesa, C. Villarreal-Garza, F. Ávila-Moreno, and O. Arrieta. 2018. Long non-coding RNAs: implications in targeted diagnoses, prognosis, and improved therapeutic strategies in human non- and triple-negative breast cancer. *Clin. Epigenetics.* 10:88. <https://doi.org/10.1186/s13148-018-0514-z>
- Son, D., Y. Kim, S. Lim, H.G. Kang, D.H. Kim, J.W. Park, W. Cheong, H.K. Kong, W. Han, W.Y. Park, et al. 2019. miR-374a-5p promotes tumor progression by targeting ARRB1 in triple negative breast cancer. *Cancer Lett.* 454:224–233. <https://doi.org/10.1016/j.canlet.2019.04.006>
- Wang, Z., D. Katsaros, N. Biglia, Y. Shen, L. Loo, X. Yu, H. Lin, Y. Fu, W.M. Chu, P. Fei, et al. 2019. ERA upregulates the expression of long non-coding RNA LINC00472 which suppresses the phosphorylation of NF- κ B in breast cancer. *Breast Cancer Res. Treat.* 175:353–368. <https://doi.org/10.1007/s10549-018-05108-5>
- Wei, D., X. Le, L. Zheng, L. Wang, J.A. Frey, A.C. Gao, Z. Peng, S. Huang, H.Q. Xiong, J.L. Abbruzzese, and K. Xie. 2003. Stat3 activation regulates the expression of vascular endothelial growth factor and human pancreatic cancer angiogenesis and metastasis. *Oncogene.* 22:319–329. <https://doi.org/10.1038/sj.onc.1206122>
- Wu, H., J. Zheng, J. Deng, L. Zhang, N. Li, W. Li, F. Li, J. Lu, and Y. Zhou. 2015. LincRNA-uc002yug.2 involves in alternative splicing of RUNX1 and serves as a predictor for esophageal cancer and prognosis. *Oncogene.* 34: 4723–4734. <https://doi.org/10.1038/nc.2014.400>
- Xia, X., X. Li, F. Li, X. Wu, M. Zhang, H. Zhou, N. Huang, X. Yang, F. Xiao, D. Liu, et al. 2019. A novel tumor suppressor protein encoded by circular AKT3 RNA inhibits glioblastoma tumorigenicity by competing with active phosphoinositide-dependent Kinase-1. *Mol. Cancer.* 18:131. <https://doi.org/10.1186/s12943-019-1056-5>
- Yan, J., Q. Wang, K. Zou, L. Wang, E.B. Schwartz, J.R. Fuchs, Z. Zheng, and J. Wu. 2015. Inhibition of the JAK2/STAT3 signaling pathway exerts a therapeutic effect on osteosarcoma. *Mol. Med. Rep.* 12:498–502. <https://doi.org/10.3892/mmr.2015.3439>

- Yang, R., L. Xing, M. Wang, H. Chi, L. Zhang, and J. Chen. 2018. Comprehensive Analysis of Differentially Expressed Profiles of lncRNAs/mRNAs and miRNAs with Associated ceRNA Networks in Triple-Negative Breast Cancer. *Cell. Physiol. Biochem.* 50:473–488. <https://doi.org/10.1159/000494162>
- Yu, X., A.Y. Abdullahi, S. Wu, W. Pan, X. Shi, W. Hu, L. Tan, K. Li, Z. Wang, and G. Li. 2017. Prokaryotic Expression of α -13 Giardin Gene and Its Intracellular Localization in *Giardia lamblia*. *BioMed Res. Int.* 2017: 1603264. <https://doi.org/10.1155/2017/1603264>
- Zhang, T., W.H. Kee, K.T. Seow, W. Fung, and X. Cao. 2000. The coiled-coil domain of Stat3 is essential for its SH2 domain-mediated receptor binding and subsequent activation induced by epidermal growth factor and interleukin-6. *Mol. Cell. Biol.* 20:7132–7139. <https://doi.org/10.1128/MCB.20.19.7132-7139.2000>
- Zhang, C.Y., M.S. Yu, X. Li, Z. Zhang, C.R. Han, and B. Yan. 2017a. Over-expression of long non-coding RNA MEG3 suppresses breast cancer cell proliferation, invasion, and angiogenesis through AKT pathway. *Tumour Biol.* 39:1010428317701311.
- Zhang, Y., D.L. Wang, H.Y. Yan, J.Y. Liao, J.H. He, K.S. Hu, W.X. Deng, Y.J. Wang, H.T. Xing, H.P. Koeffler, and D. Yin. 2017b. Genome-wide study of ER-regulated lncRNAs shows AP000439.3 may function as a key regulator of cell cycle in breast cancer. *Oncol. Rep.* 38:3227–3237. <https://doi.org/10.3892/or.2017.5975>
- Zhang, M., K. Zhao, X. Xu, Y. Yang, S. Yan, P. Wei, H. Liu, J. Xu, F. Xiao, H. Zhou, et al. 2018. A peptide encoded by circular form of LINC-PINT suppresses oncogenic transcriptional elongation in glioblastoma. *Nat. Commun.* 9:4475. <https://doi.org/10.1038/s41467-018-06862-2>
- Zhang, H., N. Zhang, Y. Liu, P. Su, Y. Liang, Y. Li, X. Wang, T. Chen, X. Song, Y. Sang, et al. 2019. Epigenetic regulation of NAMPT by NAMPT-AS drives metastatic progression in triple-negative breast cancer. *Cancer Res.* 79:3347–3359. <https://doi.org/10.1158/0008-5472.CAN-18-3418>

Supplemental material

Wang et al., <https://doi.org/10.1084/jem.20190950>

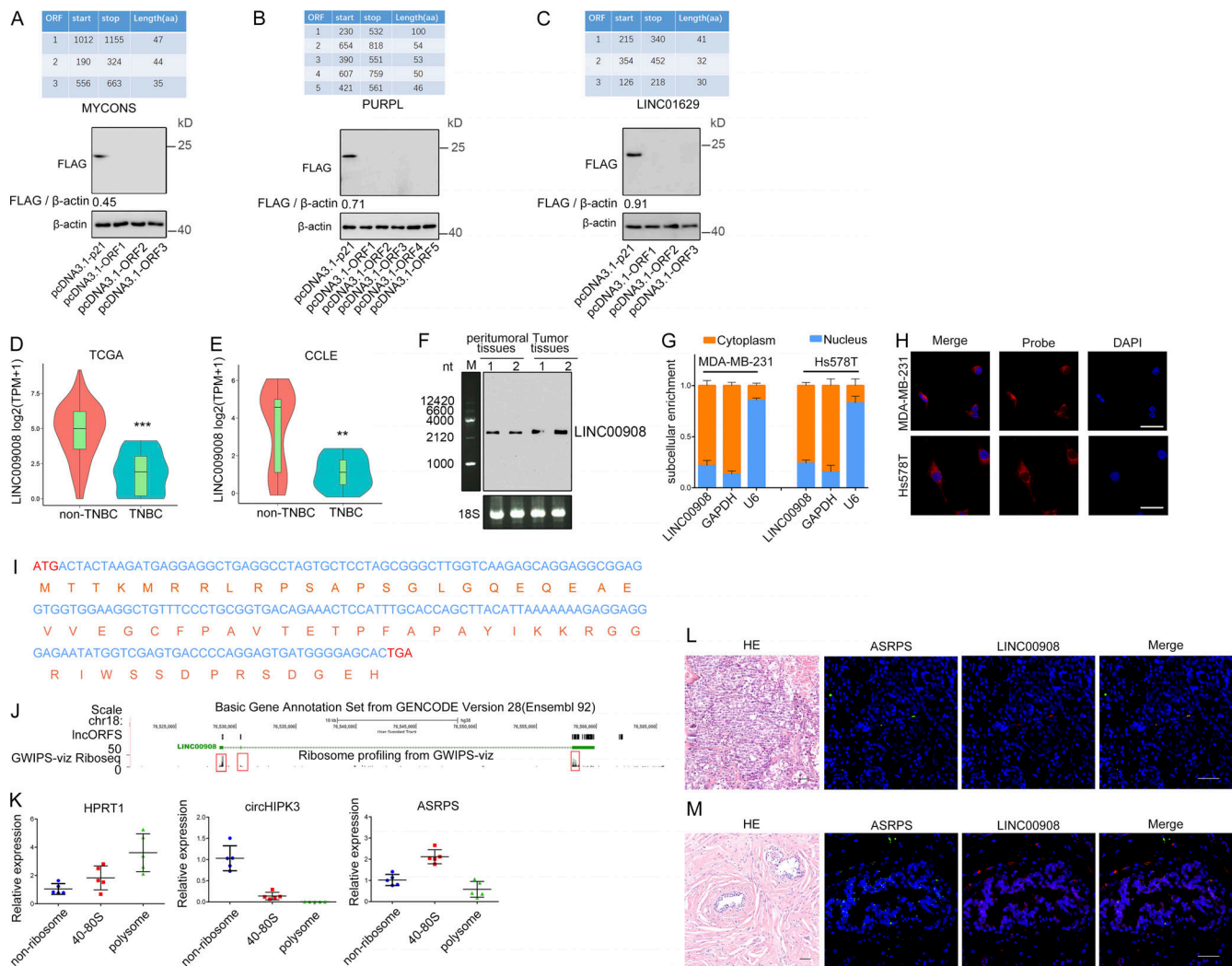


Figure S1. **Screening of candidate lncRNAs and biological characterization of *LINC00908*.** (A) The genomic position of the predicted ORFs of *MYCONS*. None of the three predicted ORFs was translated when transfected in MDA-MB-231 cells. (B) The genomic position of the predicted ORFs of *PURPL*. None of the five predicted ORFs was translated when transfected in MDA-MB-231 cells. (C) The genomic position of the predicted ORFs of *LINC01629*. None of the three predicted ORFs was translated when transfected in MDA-MB-231 cells. (D) The *LINC00908* expression level in TCGA database (TNBC, $n = 18$; non-TNBC, $n = 347$). (E) The *LINC00908* expression level in the Cancer Cell Line Encyclopedia (CCLE) project (TNBC, $n = 19$; non-TNBC, $n = 30$). (F) Northern blot analysis of *LINC00908* transcript in two pairs of matched TNBC tissue samples. M, marker. (G) The majority of *LINC00908* transcript was present in the cytoplasmic fraction of MDA-MB-231 and Hs578T cells. (H) RNA FISH analysis of *LINC00908* in MDA-MB-231 and Hs578T cells (scale bars, 50 μ m). (I) The sequence information of the peptide and the region of *LINC00908* encoding peptide. (J) Ribosome occupancy map at the *LINC00908* locus. (K) ASRPS transcript was enriched in 40S-80S and polysome fractions of MDA-MB-231 cell lysates ($n = 5$). (L) Cy3-labeled ISH probe for *LINC00908* and FITC-labeled anti-ASRPS antibody were used to detect the expression of *LINC00908* and ASRPS in tumor tissue slide (scale bar, 50 μ m). (M) Cy3-labeled ISH probe for *LINC00908* and FITC-labeled anti-ASRPS antibody were used to detect the expression of *LINC00908* and ASRPS in adjacent tumor tissue slide (scale bar, 50 μ m). Representative of three (A–M) experiments, respectively. Data are presented as the mean \pm SD. **, $P < 0.01$; ***, $P < 0.001$ by Student's t test.

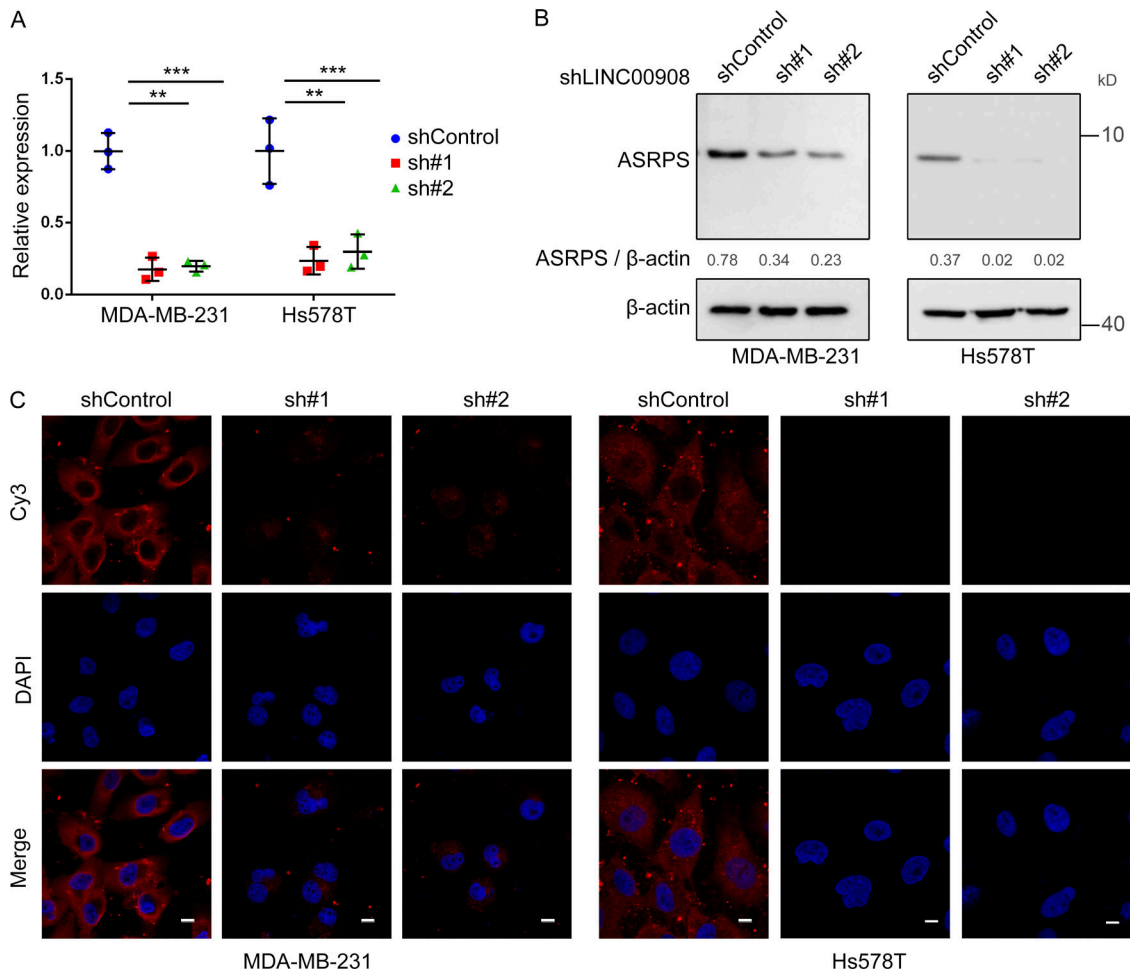


Figure S2. **Anti-ASRPS antibody specifically detects the polypeptide ASRPS.** (A) *LINC00908*-specific shRNAs significantly reduced *LINC00908* transcript in MDA-MB-231 and Hs578T cells ($n = 3$). (B) *LINC00908*-specific shRNAs significantly reduced ASRPS protein in MDA-MB-231 and Hs578T cells by Western blot analysis. (C) *LINC00908* specific shRNAs significantly reduced ASRPS protein in MDA-MB-231 and Hs578T cells by immunofluorescence staining (scale bars, 10 μ m). Representative of three (A–C) experiments, respectively. Data are presented as the mean \pm SD. **, $P < 0.01$; ***, $P < 0.001$ by Student's t test.

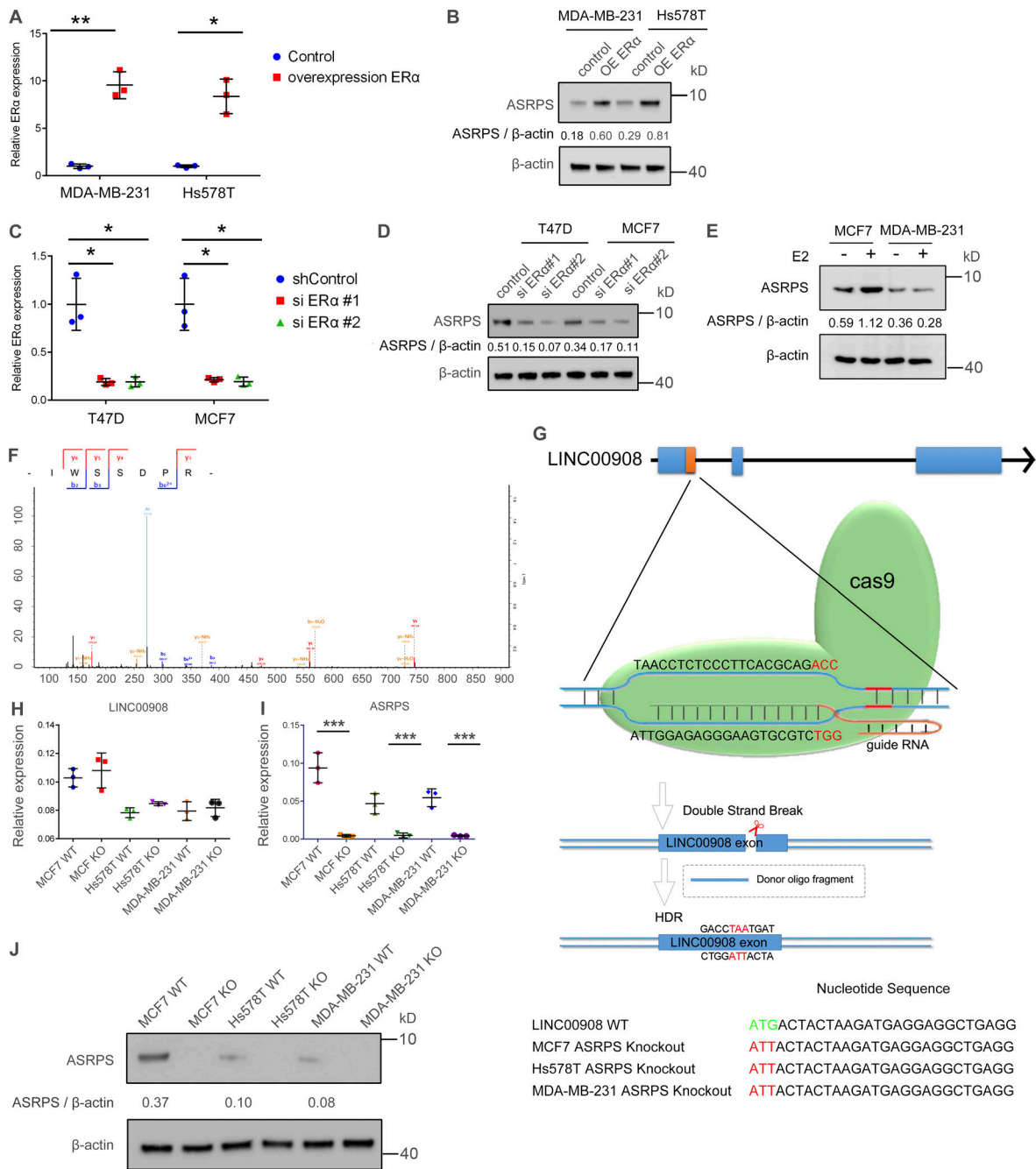


Figure S3. **Silencing and OE of ERα, mass spectrometry (MS/MS) result of ASRPS and ASRPS KO in BC cell lines.** (A) OE of ERα in MDA-MB-231 and Hs578T cells ($n = 3$). (B) The level of ASRPS was determined by Western blot. (C) Down-regulation of ERα in MCF7 and T47D cells ($n = 3$). (D) The level of ASRPS was determined by Western blot. (E) MCF7 and MDA-MB-231 cells were treated with E2, and the level of ASRPS was detected by Western blot. (F) Mass spectrometry result of ASRPS from colP with STAT3 antibody in MCF7. (G) ASRPS KO in BC cell lines using CRISPR/Cas9 system. (H) ASRPS KO did not affect *LINC00908* RNA levels in BC cell lines ($n = 3$). (I) ASRPS KO reduced levels of polypeptide ASRPS by polysome profiling ($n = 3$). (J) The level of ASRPS were determined by Western blot. Representative of three (A–J) experiments, respectively. Data are presented as the mean \pm SD. *, $P < 0.05$; **, $P < 0.01$; ***, $P < 0.001$ by Student's *t* test. HDR, homologous directed repair.

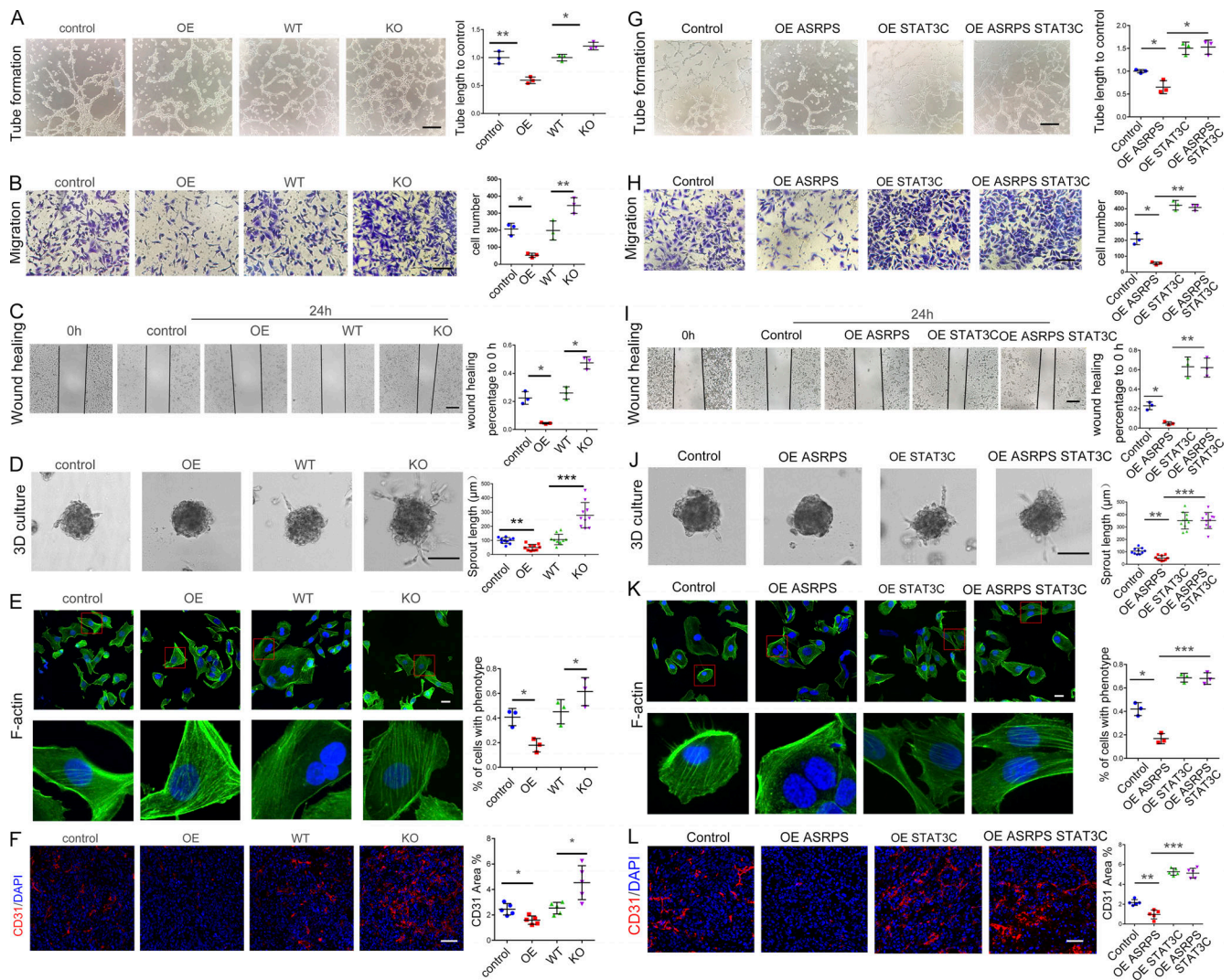


Figure S4. ASRPS affected migration, invasion, and angiogenesis in BC cell lines, but STAT3C expression fully reversed the effect of ASRPS OE. HUVECs were incubating with conditioned medium prepared from Hs578T cells with ASRPS OE, KO, STAT3C OE and ASRPS, STAT3C OE. **(A–E and G–K)** Matrigel tube formation (scale bars, 200 μm; *n* = 3; A and G), transwell migration (scale bars, 50 μm; *n* = 3; B and H), wound healing migration (scale bars, 200 μm; *n* = 3; C and I), sprouting assay (scale bars, 200 μm; *n* = 10; D and J), and cytoskeletal reorganization (scale bars, 20 μm; *n* = 3; E and K) of HUVECs. **(F)** CD31 expression in mouse BC xenograft model injected with Hs578T cells with ASRPS OE or ASRPS KO (scale bar, 50 μm; *n* = 5). **(L)** CD31 expression in mouse BC xenograft model injected with Hs578T cells with ASRPS OE, STAT3C OE and ASRPS, STAT3C OE (scale bars, 50 μm; *n* = 5). Representative of three (A–L) experiments, respectively. Data are presented as the mean ± SD. *, *P* < 0.05; **, *P* < 0.01; ***, *P* < 0.001 by Student's *t* test.

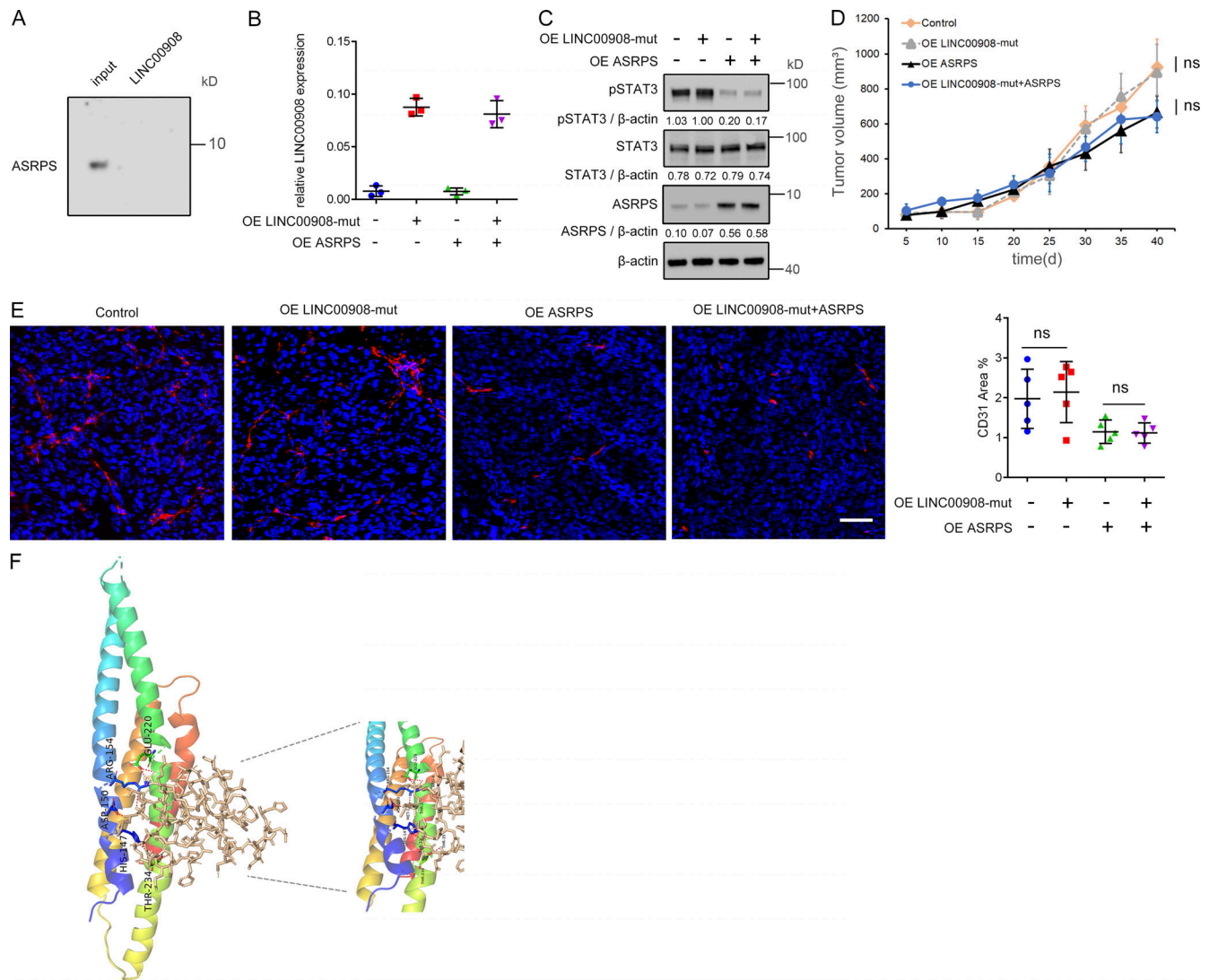


Figure S5. *LINC00908* cannot have effect on angiogenesis or reverse the effect of tumor angiogenesis caused by ASRPS. (A) Pull-down assay was performed using *LINC00908* and the eluted protein was detected by anti-ASRPS antibody. (B) Relative expression level of *LINC00908* ($n = 3$). (C) Phosphorylation of STAT3 was not rescued by *LINC00908*. (D) OE *LINC00908-mut* cannot increase tumor growth or rescue the effect on tumor growth caused by ASRPS ($n = 5$). (E) OE *LINC00908-mut* cannot increase tumor angiogenesis or rescue the effect on tumor angiogenesis caused by ASRPS (scale bar, 50 μ m; $n = 5$). (F) Molecular docking of ASRPS binding site in CCD domain. Representative of three (A–E) experiments, respectively. Data are presented as the mean \pm SD, not significant by Student's t test.

Tables S1–S5 are provided online as separate Excel files. Table S1 lists primary clinical and histological characteristics of 217 study patients. Table S2 lists virus strains and recombinant DNA used in this study. Table S3 lists antibodies used in this study. Table S4 lists primers and gRNA used in this study. Table S5 lists sequences of siRNAs and shRNAs used in this study.